ACS OMEGA

Open Access

http://pubs.acs.org/journal/acsodf

Review

Recent Advances Hydrogenation of Carbon Dioxide to Light Olefins over Iron-Based Catalysts via the Fischer−Tropsch Synthesis

Jiangtao Liu, Yongchun Zhang,* and Chong Peng*

Cite This: *ACS Omega* 2024, 9, 25610−25624

Read Online

ACCESS | Metrics & More | Article Recommendations

ABSTRACT: The massive burning of fossil fuels has been important for economic and social development, but the increase in the CO_2 concentration has seriously affected environmental sustainability. In industrial and agricultural production, light olefins are one of the most important feedstocks. Therefore, the preparation of light olefins by CO_2 hydrogenation has been intensively studied, especially for the development of efficient catalysts and for the application in industrial production. Fe-based catalysts are widely used in Fischer−Tropsch synthesis due to their high stability and activity, and they also exhibit excellent catalytic CO_2 hydrogenation to light olefins. This paper systematically summarizes and analyzes the reaction mechanism of Fe-based catalysts, alkali and transition metal modifications, interactions between active sites and carriers, the synthesis process, and the effect of the byproduct H_2O on catalyst performance. Meanwhile, the challenges to the development of CO_2 hydrogenation for light olefin synthesis are presented, and future development opportunities are envisioned.

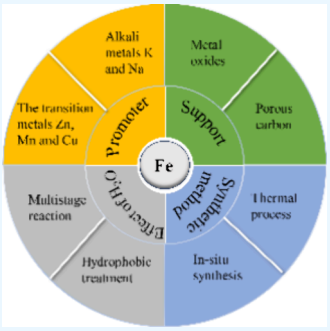

1. INTRODUCTION

In recent years, the excessive use of fuels such as oil, coal, and natural gas has greatly contributed to the development of the economy and human society, but the increasing carbon dioxide emissions in the course of development have also brought about various environmental challenges, such as the greenhouse effect, ocean acidification, and climate anomaly.[1−3] Despite CO_2 being a greenhouse gas, CO_2 is a nontoxic carbon source that provides a fungible pathway to produce high-value-added products.[4,5] The direct conversion of CO_2 into value-added products is not only conducive to alleviating environmental issues caused by excessive CO_2 emission, but also realizes the resource utilization of CO_2.[6−10] Therefore, CO_2 hydrogenation to value-added chemicals is an excellent way to reduce CO_2 concentrations and arouse the interest of researchers.[11−13]

Light olefins ($C_2^=-C_4^=$) play a vital role in industry and agriculture. In fact, light olefins as building blocks could produce a variety of chemicals, such as solvents, cosmetics, medicines, fuels, polymers, etc.[14−17] Industrially, light olefins are generally produced through processes such as steam cracking of naphtha and fluid catalytic cracking, which are not only costly, but also inefficient.[18−20] In addition, with the continuous depletion of crude oil resources and the significant demand, it is very urgent to develop a fungible way to produce light olefins.[21,22] Therefore, thermocatalytic CO_2 hydrogenation to a light olefin is an effective strategy to alleviate the environmental problem caused by excessive CO_2 emissions and also provides a way to synthesize light olefins.

With the deeper investigation of CO_2 hydrogenation for the preparation of light olefins, two reaction routes have been accepted, as shown in Figure 1:[23] (1) the methanol intermediate route (MTO): methanol is obtained by the hydrogenation of carbon dioxide, followed by methanol dehydration to obtain light olefins; (2) the CO_2 hydrogenation Fischer−Tropsch pathway (FTS): the CO_2 hydrogenation FTS route is composed of RWGS and FTS reactions, where CO_2 is first converted to CO via the reverse water−gas shift (RWGS) reaction, and then CO by the FTS route is used to synthesize light olefins.[24] The MTO route is not affected by the ASF distribution and, as a result, has higher light olefin

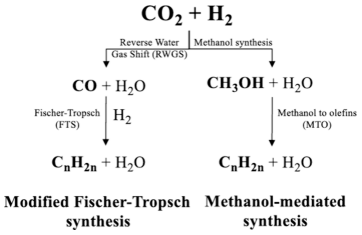

Figure 1. Route to CO_2 hydrogenation for the production of light olefins. Reproduced with permission from ref 23. Copyright 2019 Wiley.

Received: March 31, 2024
Revised: May 21, 2024
Accepted: May 24, 2024
Published: June 6, 2024

selectivity. The temperature at which carbon dioxide is converted to methanol and methanol to low-carbon olefins is different in the MTO reaction process.[25] Thermodynamically, high temperatures (400−450 °C) are beneficial for methanol dehydration to prepare low-carbon olefins, but high temperatures are advantageous for CO_2 to produce CO rather than methanol via the RWGS reaction.[26−28] Therefore, for the MTO route, low-temperature kinetics and high-temperature thermodynamics limit the yield of both methanol and light olefins. For the FTS route, the RWGS conversion of CO plays a vital role in the downstream FTS step to light olefins. The RWGS reaction is adsorptive, whereas the FTS reaction is exothermic, which gives FTS a thermodynamic advantage over MTO.[23] CO_2-FTS with excellent RWGS performance and high toxicity resistance requires relatively low feed gas composition and purity and has a wider temperature operating range, which makes it suitable for carbon-rich feed gas produced by coal or biomass gasification.[29] Moreover, CO_2-FTS is mainly a Fe-based catalyst, which is less expensive than Co and Ru catalysts.[30]

Because CO_2-FTS shares a common reaction process with conventional CO-FTS, the design and application of CO_2−FTS catalysts follow the strategy of the CO-FTS catalysts. Co-based and Fe-based catalysts have a wide range of applications in CO-FTS. The Co-based catalysts, however, have low RWGS activity during the CO_2-FTS reaction, and the high ability of Co for active CO hydrogenation leads to the outstanding selectivity of CH_4 in the product.[2,30] Fe-based catalysts have higher RWGS and FTS reactivity and catalytic stability; in addition, Fe-based catalysts have better C−C coupling during CO_2 hydrogenation, which is also favorable for the preparation of low-carbon olefins.[22,31,32] Usually, the products of catalyzed CO_2 hydrogenation over Fe-based catalysts obey the Anderson−Schulz Flory (ASF) law, as shown in Figure 2.[33]

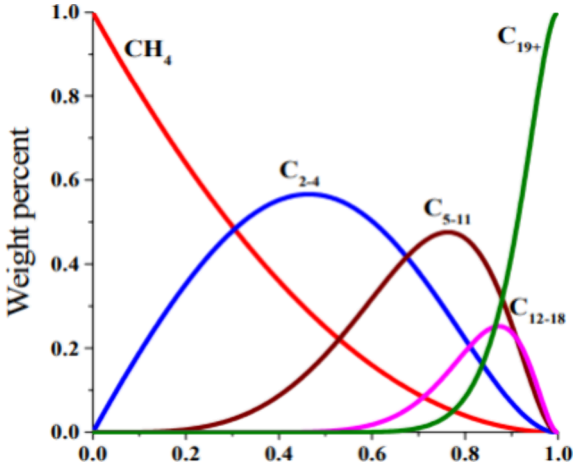

Figure 2. ASF model of product distribution for Fischer−Tropsch synthesis. Reproduced with permission from ref 33. Copyright 2017 Royal Society of Chemistry.

To improve the selectivity of light olefins, the morphology, crystal structure, reduction, and adsorption capacity of Fe-based catalysts were modulated by adjusting the preparation method of Fe-based catalysts, the conditions of pretreatment, and the catalyst carrier to improve the selectivity of light olefins.

Recently, with the growing interest in CO_2 hydrogenation to light olefins, it is important to design multifunction catalysts to achieve the synthesis of light olefins more efficiently.[34,35] Thus, it is necessary to conclude the recent progress and general trends of CO_2 hydrogenation to light olefins. In this Review we mainly introduce reaction routes (CO_2-FTS) for the hydrogenation of CO_2 to produce light olefins. For the (CO_2-FTS pathway), we discuss general trends in a few important aspects: (1) the reaction mechanism and (2) the catalyst design concepts (catalysts and active phases, alkali metals, bimetallic catalysts, and catalyst carriers). We hope that the perception provided in this Review will promote the development of CO_2 hydrogenation to light olefins in thermocatalytic systems.

2. REACTION MECHANISMS

The CO_2 Fischer−Tropsch routes consist of two consecutive processes to synthesize light olefins, the RWGS reaction, and FTS. The relevant equations are as follows:[2]

RWGS:

$$CO_2 + H_2 \rightarrow CO + H_2O;\ \Delta rH_m^0/ = +41.1\ kJ{\cdot}mol^{-1}$$

FTS:

$$2CO + 4H_2 \rightarrow C_2H_4 + 2H_2O;\ \Delta rH_m^0/ = -210.2\ kJ{\cdot}mol^{-1}$$

$$3CO + 6H_2 \rightarrow C_3H_6 + 3H_2O;\ \Delta rH_m^0/ = -373.6\ kJ{\cdot}mol^{-1}$$

$$4CO + 8H_2 \rightarrow C_4H_8 + 4H_2O;\ \Delta rH_m^0/ = -402.2\ kJ{\cdot}mol^{-1}$$

Due to the two-step reaction process of RWGS and FTS in the catalytic CO_2 hydrogenation process, the Fe-based catalysts also have the corresponding catalytically active phases in different reaction processes. For the Fe catalysts, during the reaction, Fe_2O_3 first undergoes a phase transition to form Fe_3O_4, which is then reduced to FeO and Fe, ultimately forming catalytically active Fe_xC, as seen in Figure 3.[36−38]

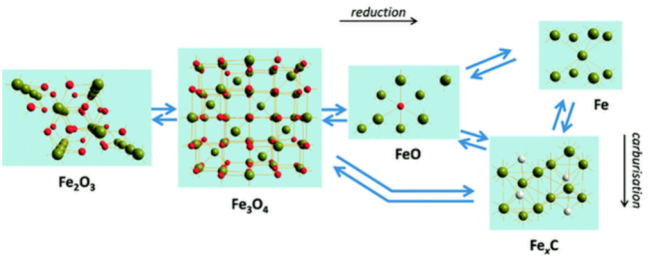

Figure 3. Schematic diagram of the phase transition of Fe during hydrogenation of CO_2-FTS. Reproduced with permission from ref 38. Copyright 2018 Royal Society of Chemistry.

For the RWGS reaction, three main reaction routes are included, as shown in Figure 4a:[38,39] the direct dissociation mechanism (CO_2* → CO* + O*), the COOH* mediate mechanism (CO_2* + H* → COOH*), and the HCOO* mediate mechanism (CO_2* + H* → HCOO*).[40] The dissociation of CO_2 into O* and CO* is promoted due to the easy interaction of O* with Fe and iron carbide, as seen in Figure 4b−d.[41] When Fe-based catalysts are present in the form of Fe_3O_4 and Fe_2O_3, their alkaline properties promote CO_2 adsorption and inhibit direct CO_2 dissociation. HCOO* intermediates are easily formed on Fe_3O_4 surfaces, and lower energies are required for the formation of COOH* intermediates on Fe_2O_3 surfaces (Figure 4e,f).[42−44] However, the subsequent dissociation of either HCOO* and COOH* intermediates occurring to form CHO* and CO* requires

https://doi.org/10.1021/acsomega.4c03075
ACS Omega 2024, 9, 25610−25624

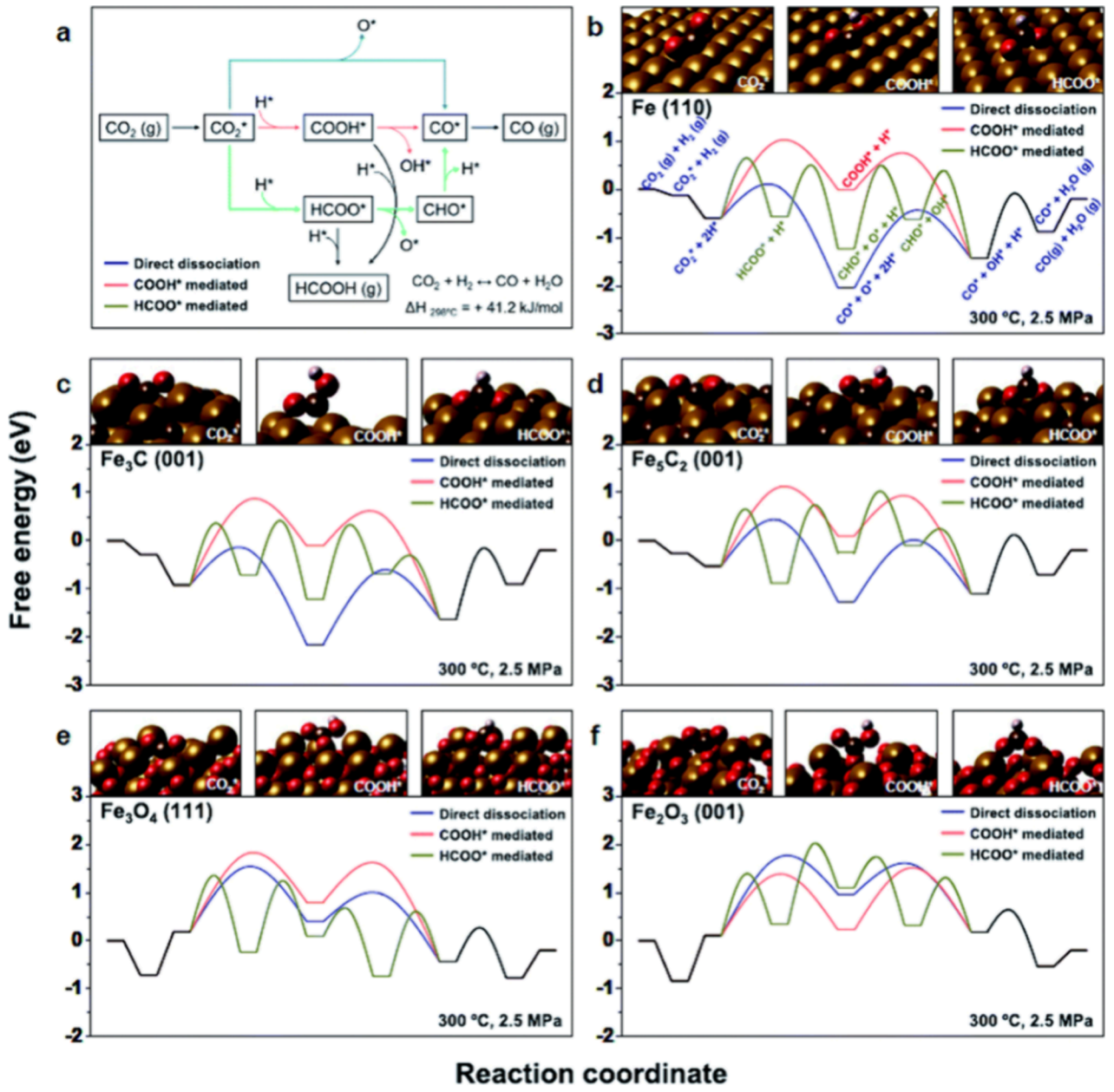

Figure 4. (a) Reaction pathways for the reverse water−gas shift (RWGS) reaction. Relative energy diagrams for CO_2 hydrogenation via the dissociation mechanism (blue), the COOH*-mediated mechanism (orange), and the HCOO*-mediated mechanism (green). (b) Fe (110), (c) Fe_3C (001), (d) Fe_5C_2 (001) surface, (e) Fe_3O_4 (110), and (f) Fe_2O_3 (001) surfaces. Reproduced with permission from ref 41. Copyright 2020 Royal Society of Chemistry.

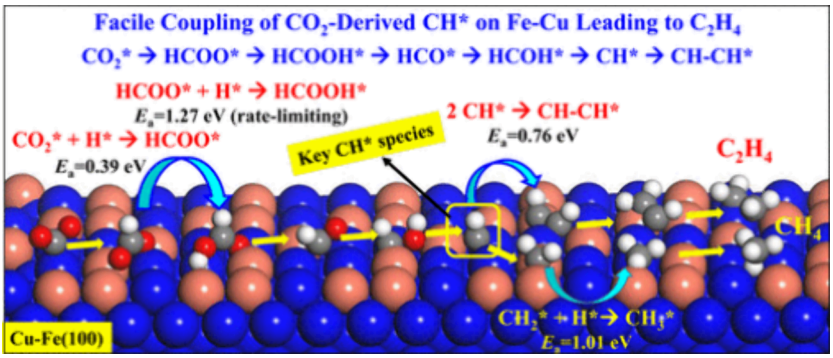

Figure 5. Proposed reaction mechanism of CO_2 hydrogenation to CH_4 and C_2H_4 over Cu−Fe bimetallic surfaces by DFT calculations. Reproduced with permission from ref 58. Copyright 2017 American Chemical Society.

https://doi.org/10.1021/acsomega.4c03075
ACS Omega 2024, 9, 25610−25624

Table 1. Summation of Fe-Based Catalysts Used for CO_2 Hydrogenation to Light Olefins

			selectivity of hydrocarbons (%)				reaction conditions				
catalysts	CO_2 con. (%)	CO sel. (%)	CH_4	$C_2^0-C_4^0$	$C_2^=-C_4^=$	C_5^+	temp (K)	P (MPa)	H_2/CO_2	GHSV (mL g^{-1}/h^{-1})	ref
Fe_3O_4	27.0	35.9	43.2	33.9	5.7	17.2	613	1.0	3	4800	64
Na-Fe	33.0	20.9	20.7	4.5	24.4	50.7	613	1.0	3	4800	64
Fe_3O_4-NaAc	30.4	18.5	12.0	4.5	29.3	54.2	593	0.5	3	560	65
1.18Na-Fe	40.5	13.5	15.8	7.5	46.6	30.1	593	3.0		2000	66
K-Fe	38	7.3	21	14	34	30	613	2	3	2700	67
0K-Fe	30.0	15	40	23	15	7	593	2.0	3	N/A	68
2K-Fe	30.0	22.0	23	15	24	16	593	2.0	3	N/A	68
4K-Fe	30.0	22	6	15	24	33	593	2.0	3	N/A	68
2Na-Fe-Zn	43.0	15.7	22.8	7.4	54.1	7.4	593	1.5	3	1000	69
K-Fe-Zn	51.0	6.0	34.9	7.8	53.6	3.7	593	2.0	3	1000	70
K-Fe-Zn/NC	34.6	21.2	24.2	7.1	40.6	28.1	593	3.0	3	7200	71
K-Fe-Zr	54.4	3	19.8	8.3	53.6	18.3	593	2.0	3	1000	72
K-Fe-Zr-Ce	57.3	3.1	20.6	7.9	55.6	15.9	593	2.0	3	1000	72
10K-Fe_2O_3/Al_2O_3	24.1	23.4	7.5	3.4	25.3	40.4	593	3.0	3	3600	73
10K-Fe_5C_2/Al_2O_3	31.5	18.6	12.1	4.4	35.8	29.1	593	3.0	3	3600	73
K-10Fe/m-ZrO_2	40.5	17.0	N/A	N/A	15.0	N/A	613	2.0	4.0	N/A	74
K-10Fe/t-ZrO_2	22.3	N/A	N/A	N/A	10.9	N/A	613	2.0	4.0	N/A	74
K-Fe-Cr/Nb_2O_5	31.0	57.0	32.0	1.0	10.0	57.0	723	1.0	3.0	3600	75
K-Fe-Zn/NC	34.6	21.2	24.2	7.1	40.6	28.1	593	3.0	3.0	7200	76
Na-$CoFe_2O_4$/CNTs	34.4	19.0	5.0	18.0	38.8	40.9	613	3.0	3.0	3600	77
Na-$CoFe_2O_4/TiO_2$	17.9	42.8	66.2	12.9	17.2	3.7	613	3.0	3.0	3600	77

higher energies, which is detrimental to the continuation of the RWGS reaction.[12,45−47] Therefore, during the CO_2-FTS reaction, high-temperature H_2 reduction of iron oxides were carried out prior to the reaction to reduce the amount of Fe_2O_3 that was not catalytically active.

C−C coupling is a key step in the formation of multicarbon olefins by CO_2 hydrogenation.[17,48] In the case of hydrocarbons, CO* species are first hydrogenated to HCO* and then undergo a series of hydrogenation and decomposition processes to form CH_x* substances, which are the building blocks for the formation of low-carbon olefins.[49−52] The reaction mechanism in Figure 5 indicates that CH* undergoes a competitive reaction between methane and ethylene during hydrogenation.[53−55] CH_4 is formed when the resulting CH* is first subjected to a sequential hydrogenation reaction; conversely, CH* is coupled to C−C to form C_2H_2*, and then C_2H_2* is hydrogenated to form C_2H_4.[56−59] The authors found that sequential hydrogenation of CH* on Fe-based catalysts requires higher energy compared to C−C coupling of CH*, and thus, the process inhibits CH_4 formation and improves C_2H_4 selectivity.[59]

In summary, FTS-CO_2 hydrogenation for direct synthesis of light olefins mainly consists of RWGS and FTS reactions in which CO_2 is first converted to CO by RWGS reaction, and then the generated CO is further converted to olefins by the FTS reaction. Various in situ characterization techniques and DFT have been used to reveal the reaction mechanism of the CO_2-FTS pathway hydrogenation to olefins, however, the intermediate species and reaction pathways during CO_2 hydrogenation over Fe-based catalysts still need to be further explored.

3. FE-BASED CATALYSTS

During the CO_2-FTS reaction, RWGS plays a decisive role in CO formation and FTS influences the distribution and selectivity of low-carbon olefins. Generally speaking, conventional Fe-based catalysts are poorly suited to catalyze CO_2 hydrogenation for the preparation of light olefins.[60] In order to increase the selectivity of light olefins, a series of improved methods have therefore been derived for Fe-based catalysts.[61−63] Here, this paper reviewed the effects of alkali metal promoters, transition metal promoters, carriers, preparation methods, and byproduct H_2O on Fe-based catalysts. In Table 1, the results of recent studies on CO_2-FTS are summarized.

3.1. Fe-Based Catalyst Active Phase. In multiphase catalytic systems, the composition of the catalyst active centers and their relative contents have a great influence on the reaction rate and product selectivity.[78−80] Fe-based catalysts were utilized for the CO_2 hydrogenation reactions with high selectivity for both $C_2-C_4^=$ and C_5^+ in the products. The main component of Fe in the Fe-based catalysts used for CO_2 hydrogenation is iron oxide. The main forms of iron oxides present are hematite (α-Fe_2O_3), magnetite (γ-Fe_2O_3), magnetite (Fe_3O_4), and tungsten−titanium ore (FeO).[81] Zhang et al.[82] used tests such as operando Raman spectroscopy (ORS) and X-ray diffraction (OXRD) coupled with online gas chromatography (GC), as well as ex-situ characterization methods of (sub)surface structures of iron-based catalysts before and after CO_2 hydrogenation, have been applied to explore the structure evolution of iron active phases. As shown in Figure 6a, the phase transformation of α-Fe_2O_3 (γ-Fe_2O_3) during CO_2 hydrogenation was changed to α-Fe_2O_3 (γ-Fe_2O_3) → α-Fe_3O_4 (γ-Fe_3O_4) → α-Fe (γ-Fe) → χ-Fe_5C_2 (θ-Fe_3C). The adsorption capacity for CO_2 and the hydrogenation capacity of iron carbides with different structures are significantly different. Not only does χ-Fe_5C_2 require higher energy for C−C coupling, but it also has a weaker ability to bind H_2, which results in a product with a higher selectivity for low-carbon olefins. It is analyzed by CO_2-TPD that θ-Fe_3C has a high CO_2 chemisorption capacity, which is conducive to efficient C−C coupling of CO_2 on the surface of θ-Fe_3C, and thus, the selectivity of C_5^+ in the product is high. Therefore, χ-Fe_5C_2 is more selective for light olefins, but less selective for C_5^+ compared to θ-Fe. Because of the different catalytic effects

https://doi.org/10.1021/acsomega.4c03075
ACS Omega 2024, 9, 25610−25624

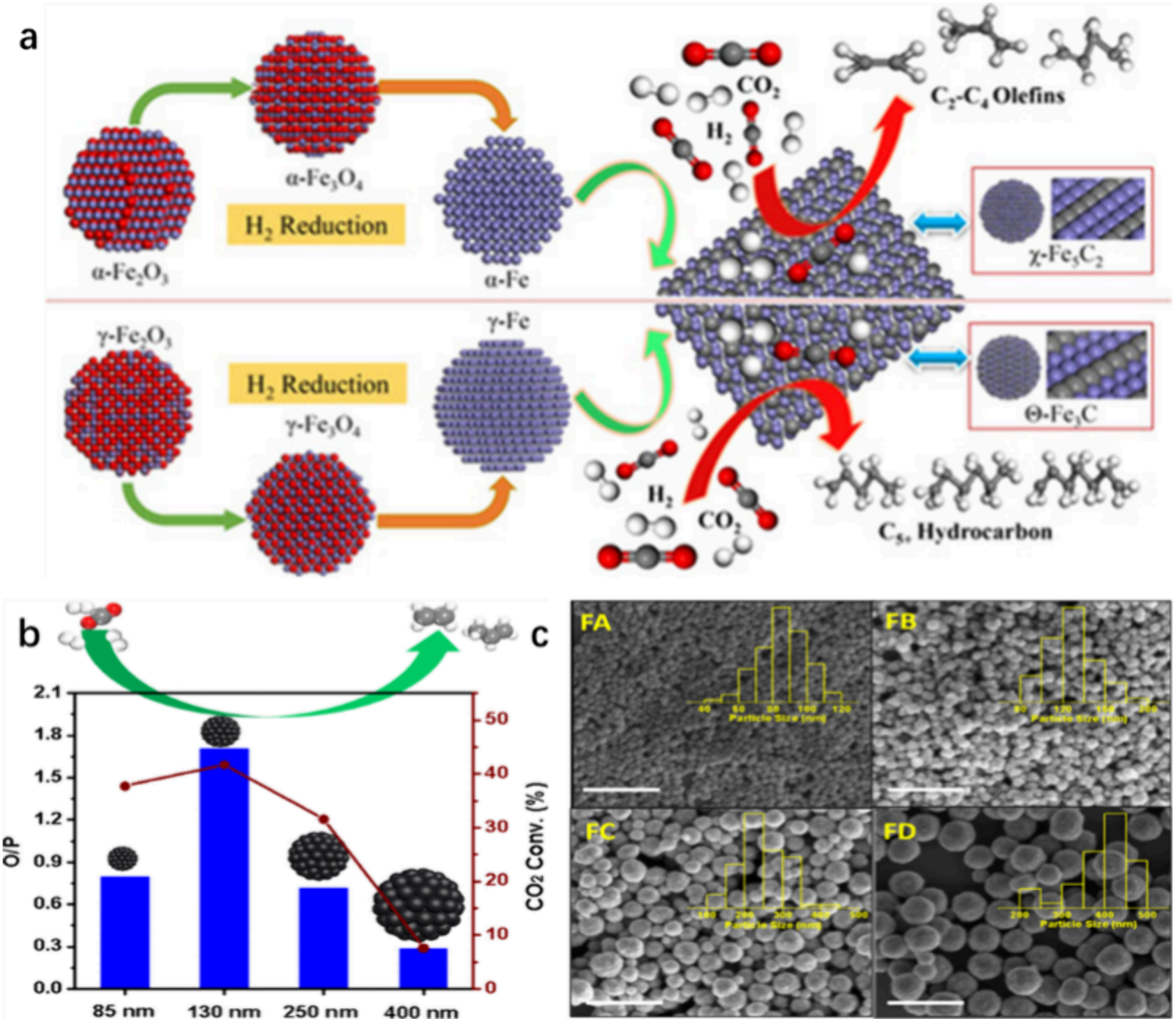

Figure 6. (a) Effect of carbonation on relative product selectivity for different Fe. Reproduced with permission from ref 82. Copyright 2018 Wiley. (b) Reaction results of catalysts of different sizes; (c) SEM of catalysts of different sizes. Reproduced with permission from ref 87. Copyright 2021 American Chemical Society.

of Fe_5C_2 and Fe_3C for CO_2 hydrogenation, Fe_5C_2 and Fe_3C can be synthesized with different structures by adjusting the reduction atmospheres of Fe-based catalysts.[83] Tang et al.[84] had gained an in-depth understanding of the structural evolution mechanism of Fe-based catalysts under different heat treatment atmospheres by in situ analysis and found that the Fe-based catalysts would undergo deoxygenation, carburization, hydrogenation, and carbon-accumulation under a reducing atmosphere and that the Fe_5C_2 active phase was formed after the Fe catalysts underwent the reduction and carburization reaction when H_2 was used as the reducing gas. Wang et al.[85] found that FeO_x carburization that can be induced through PdFe alloys, so PdFe oxide catalysts were prepared by hydrothermal and impregnation methods, and then a PdFe alloy-Fe_5C_2 catalyst was prepared using H_2 thermal reduction. Liu et al.[86] found that the reducing gas can affect the phase transition from iron oxide to FeC_x, and the H_2/CO_2 mixture can promote the in situ formation of Fe_3C on Fe-based catalysts, and experiments have shown that the overoxidation or reduction of Fe-based catalysts can be avoided when the H_2/CO_2 ratio is 2, which can lead to the in situ formation of Fe_3C.

During CO_2 hydrogenation, the impact on the RWGS reaction process is not only related to the content of Fe_3O_4 in Fe-based catalysts, but also, the particle size of Fe_3O_4 plays a crucial role. Liu et al.[87] synthesized Fe_3O_4 nanoparticles with different particle sizes, as shown in Figure 6c, using a hydrothermal method and investigated the effects of reduction and carburization on the catalytic performance of Fe-based catalysts in the catalytic CO_2 hydrogenation process. In situ XRD of larger particle sizes of Fe_3O_4 requires more reduction time at the same temperature, and H_2-TPR indicates that the $Fe_2O_3 \rightarrow Fe_3O_4$ and $Fe_3O_4 \rightarrow Fe$ processes require higher temperatures as the particle size increases. As a result, nanoparticles of Fe_3O_4 with larger particle sizes are difficult to reduce, which affects the carburization of Fe and therefore

https://doi.org/10.1021/acsomega.4c03075
ACS Omega 2024, 9, 25610−25624

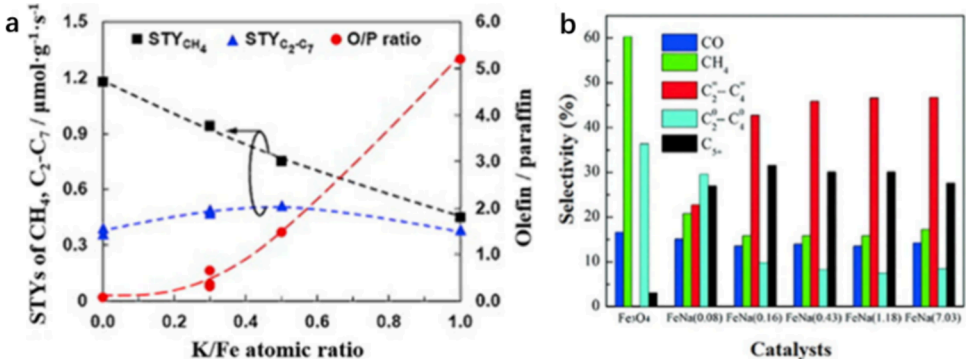

Figure 7. (a) Site-time yield (STY) of CH_4 and C_2-C_7 hydrocarbons, as well as the olefin/paraffin ratio of C_2-C_4 hydrocarbons over Fe−Co (0.17)/K(Y)/Al_2O_3 catalysts with different K/Fe atomic ratios. Reproduced with permission from ref 94. Copyright 2013 Elsevier. (b) CO and hydrocarbon selectivity over FeNa(x) catalysts with different amounts of Na. Reproduced with permission from ref 66. Copyright 2016 Royal Society of Chemistry.

reduces the conversion of CO_2. As shown in Figure 6b, when the Fe_3O_4 nanoparticle size is 130 nm, the highest conversion of CO_2 is 41.7%, the selectivity of $C_2^=-C_4^=$ is 24.6%, and the selectivity of O/P (olefins/paraffinic) is 1.71.

In summary, iron carbide is an active phase in the CO_2-FTS chain growth process. Different crystalline Fe_2O_3 forms different crystalline iron carbide after reduction and carburization, and often the Fe_5C_2 formed is more favorable for CO_2 hydrogenation to light olefins.

3.2. Alkali Metal Promoters. As reported above, Fe_3O_4 was the active phase mainly responsible for RWGS; and the metallic iron carbides and Fe could activate CO and produce hydrocarbons. However, controlling hydrocarbon chain growth to synthesize the target product ($C_2^=-C_4^=$) is a challenge due to the Anderson−Schulz−Flory (ASF) distribution, limiting the product selectivity.[88] Alkali metal doping onto Fe catalysts is an effective method to enhance the selectivity of light olefins.[89,90]

As a molecular acid gas, CO_2 prefers to absorb electrons during the catalytic process. Alkali metals are efficient electron donors that increase the alkalinity of the catalyst surface, thereby achieving the adsorption of CO_2 with the catalyst.[91] In addition, the electron-donating properties of Na and K metals make the catalysts less electrophilic, resulting in a lower hydrogen adsorption capacity increasing the C/H ratio of the catalysts and inhibiting the hydrogenation of light olefins to alkanes.[92,93] For example, Figure 7a[94] and b[66] show that with the increase of K/Fe from 0 to 1.0, the olefin/alkane ratio also followed, and the selectivity of CH_4 in the product was significantly reduced. Wang et al.[95] investigated the effects of five alkali metals for CO_2 hydrogenation on the catalytic activities of Fe/ZrO catalysts. It was reported that Li-modified Fe-based catalysts have an inhibiting effect on RWGS and FTS reactions. The other alkali metals, Na, K, Rb, and CS, observably decreased the selectivity of CH_4 and light paraffins and significantly increased the selectivity of olefins. Meanwhile, the promotion of Fe-based catalysts by Na, K, and CS increased the conversion of CO_2 as a result of the alkalinity effect of Na, K, and CS. They also found that another function of alkali metals is to promote the generation of the Fe_5C_2 phase, which is the catalytically active site in the FTS route.

K not only increases the alkalinity of the Fe catalyst surface, but also has a hydrogen-sparing effect, thus improving the selectivity of light olefins. Furthermore, different K salts have distinguished catalytic effects on the catalytic hydrogenation of CO_2. Han et al.[96] indicated that K_2SO_4, KCl, and K_2CO_3 have different effects on the formation of the χ-Fe_5C_2 active phase, as seen in Figure 8a,b. The Fe phase of the K_2SO_4-modified

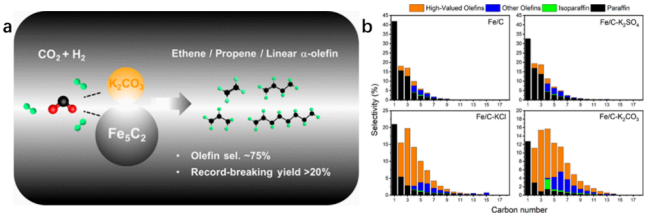

Figure 8. (a) Diagram of reaction of CO_2 hydrogenation to light olefin. (b) Product distribution of various K-modified catalysts. Reproduced with permission from ref 96. Copyright 2020 American Chemical Society.

Fe-based catalysts was mainly Fe_3O_4, indicating that K_2SO_4 was not able to promote the formation of active iron carbide in the Fe-based catalysts; Although the KCl-modified Fe-based catalysts formed Fe_5C_2, KCl did not form an agglomerated particle structure with Fe_5C_2; the K_2CO_3-modified Fe-based catalysts formed a unique $Fe_5C_2-K_2CO_3$ interface. The $Fe_5C_2-K_2CO_3$ interface in Fe/C catalysts promoted potassium to iron electron transfer to increase olefin selectivity. That enabled the Fe/C−K_2CO_3 catalyst to achieve a CO_2 conversion of 32.4% and an increase in the total olefin yield from 19.0% to 74.3%. Numpilai et al.[97] incorporated K into Fe−Co/Al_2O_3 catalysts by equipotential impregnation to promote the selection of light olefins. With the introduction of K, the increased alkalinity of the Fe catalyst surface promoted CO_2 adsorption and dissociation and inhibited the alkylation of low-carbon olefins. When the content of K reaches 0.5 wt %, the olefin/alkane (O/P) ratio is increased by 24.5 times. Jiang et al.[98] examined the catalytic properties between K and Fe−Mn catalysts by in situ Raman reflectance FTIR, and they found that K can promote the formation of metal clusters from Fe, but an excessive amount of K can mask Fe clusters to reduce the catalytic performance. You et al.[67] found that the presence of K promotes the formation of Fe_5C_2 phase on Fe-based catalysts, which facilitates CO_2 adsorption and activation, and they were also amused to find that when the content of K in the catalysts exceeds 5%, the excess of K poisons the active sites on the surface of the catalysts and reduces the catalytic reaction activity.

https://doi.org/10.1021/acsomega.4c03075
ACS Omega 2024, 9, 25610−25624

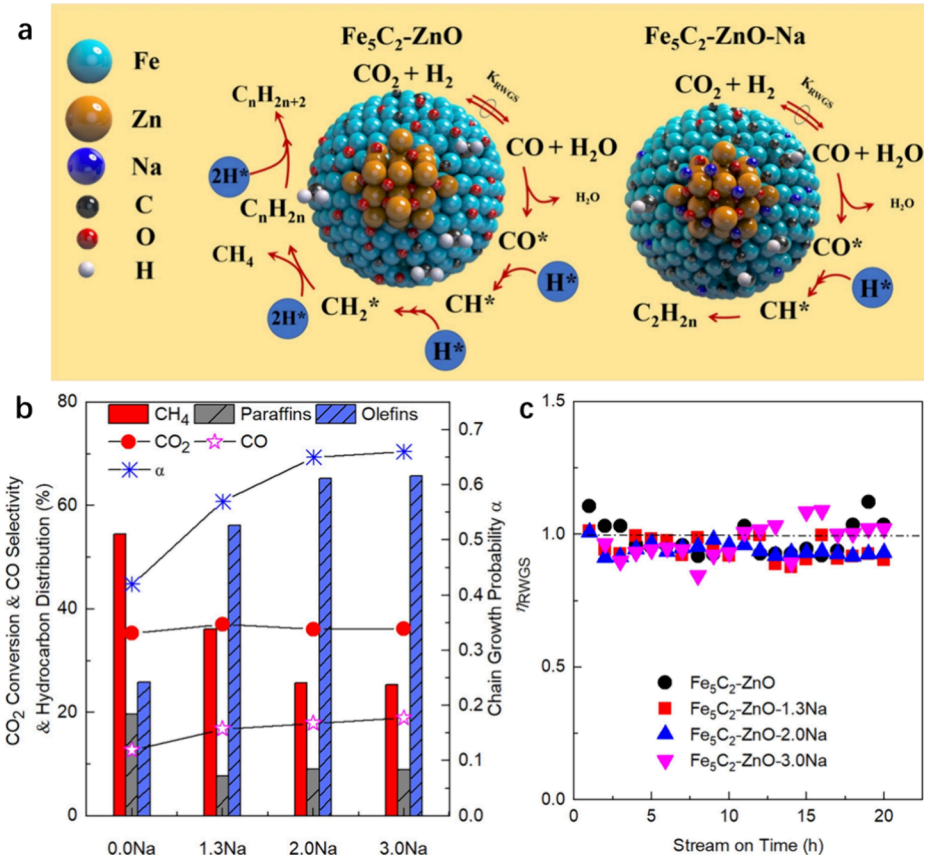

Figure 9. (a) Plausible mechanism of Na effects on Fe_5C_2 for CO_2 hydrogenation. (b) Conversion of CO_2 and carbon selectivities toward CH_4, CO, $C_2^=-C_7^=$ paraffins, and $C_2^=-C_7^=$ olefins during CO_2 hydrogenation over $Fe_5C_2-ZnO-x$Na catalysts. (c) The approach-to-equilibrium values (RWGS) for the RWGS reaction during CO_2 hydrogenation over the bimetallic Fe_5C_2-ZnO catalyst decorated with different amounts of Na. Reproduced with permission from ref 100. Copyright 2021 Elsevier.

Similar to K, Na is an alkali metal that is frequently used in Fe catalysts. Na accelerates the dissociation of light olefins and avoids the secondary hydrogenation of carbon olefins to alkanes.[99] Tu et al.[100] investigated in-depth phase transition studies for Na-modified Fe_5C_2-ZnO catalysts, as shown in Figure 9a–c. They found that Na plays an important role in inhibiting the oxidation of Fe_5C_2 and improves the stability of the Fe_5C_2 phase. In addition, Na promoted the activation of CO* and H* by altering the alkalinity of the Fe_5C_2-ZnO catalyst surface, facilitating the coupling of CH* intermediates to generate low-carbon olefins. Meanwhile, Liang et al.[101] also indicated that Na not only promotes the adsorption of CO_2 over Fe catalysts, but also has the advantage of improving the stability of Fe_5C_2 and inhibiting the hydrogenation for light olefins. Wei et al.[102] investigated the effect of Na content on the selectivity of low-carbon olefins, and when the Na content was increased from 0 to 0.5 wt %, the ratio of olefins to alkanes increased dramatically from 0.7 to 5.67. In situ Raman spectroscopy and in situ XRD showed that Na can enhance the stability of Fe_5C_2 by inhibiting the secondary hydrogenation of intermediate products to alkanes.

In summary, alkali metals K and Na are commonly used as promoters for Fe-based catalysts. K can increase CO_2 activation through alkalinity and avoid secondary hydrogenation of olefins through hydrophobicity; Na can inhibit the oxidation of Fe_5C_2 to improve the stability of the catalysts, and Na can accelerate the dissociation of light olefins to increase the olefin yield.

3.3. Transition metal promoters.

Another way to improve the CO_2 conversion and selectivity of light olefins is to add secondary metals such as Zn, Mn, and Cu, which can increase the dispersion of active centers to increase the active sites of the catalyst.

Zn as an electron-donating group can increase the alkalinity on the surface of Fe-based catalysts, thus improving the adsorption and activation of CO_2 and inhibiting the secondary hydrogenation of olefins; Second, the stronger interaction between Fe and Zn improves the degree of iron dispersion and prevents the aggregation of iron species to increase the number of active sites of iron catalysts.[103] Liu et al.[104] investigated the role of Zn for iron-based catalysts in CO_2 hydrogenation to olefins. It was found that Zn could inhibit the further oxidation of active phase Fe_5C_2 and carbon deposition on the catalyst surface during CO_2 hydrogenation, thus enhancing the long-term stability of the catalysts, and Zn could promote the adsorption of oxygen atoms on the surface and the desorption of H_2O during hydrogenation, thus reducing the possibility of oxidation of the surface carbons. Yang et al.[105] found that Zn promoted the formation of Fe_3O_4 and Fe_5C_2 reactive phases, and the ZnO/Fe_5C_2 reactive phase facilitated olefins to be easily solubilized on Fe–Zn catalysts, inhibited the secondary hydrogenation reaction of olefins, and resulted in the selectivity of light olefins of 36.9%. Zhang et al.[106] explored the reaction model of ZnO for Fe-based catalysts, as seen in Figure 10. CO_2 and H_2 were first reactivated on the surface of ZnO to produce CO_2* and H_2*, then CO_2* was reduced to

https://doi.org/10.1021/acsomega.4c03075
ACS Omega 2024, 9, 25610−25624

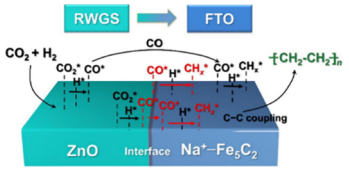

Figure 10. Reaction mechanism for CO_2 hydrogenation to olefins over the Na−Zn−Fe catalyst. Reproduced with permission from ref 106. Copyright 2021 Elsevier.

form CO* and H*, and then H* reacted with OH* to produce water. CO* undergoes a C−C coupling reaction with H* via diffusion on the surface of Na−Fe_5C_2 to form a low-carbon olefin. Meanwhile, the selectivity of olefins remained almost unchanged when the Zn content was increased from 0 to 28 wt %, while the selectivity of olefins in the products decreased significantly with the further increase of Zn content and the selectivity of CH_4 and C_2−C_4 alkanes increased. Zhang et al.[107] investigated the effect of Fe−Zn bimetallic interaction on linear α-olefins by in situ XPS characterization, showing that Zn promotes Fe reduction through electron-donating interaction. In addition, they found that the content of Zn in the catalyst could affect the ratio of FeC_x/FeO_x and thus regulate the RWGS and FTS interactions. The yield of C_2−C_4 olefins in the catalyzed product was 47.3% when the Fe/Zn molar was 2, which was 2.4 times higher than that of Fe_2O_3 catalysts.

Mn can promote the dispersion of Fe and thus effectively improve the efficiency of the CO_2 hydrogenation for the synthesis of light olefins. Moreover, the interaction between Fe and Mn species accelerated the RWGS and C−C coupling, which was attributed to the Mn promoter facilitating the transition from the Fe_3O_4 phase to the Fe_5C_2 phase in the FTS reaction, separately.[108] In addition, the interaction of Fe and Mn could weaken the carbon chain growth and improve the selectivity of light olefins.[65,109] Fedorov et al.[110] performed a detailed experimental analysis of the reaction pathway of CO_2 hydrogenation on Fe catalysts, and Fe-based catalysts undergo not only RWGS and FTS reactions, but also methanation. When the chain growth probability is lower than 0.18, the active site has higher CH_4 selectivity, and when transition metal Mn is doped in the Fe-based catalysts, the methanation of the Fe-based catalysts can be effectively inhibited, thus improving the chain growth ability of the catalysts. Due to the low light olefin selectivity of traditional Fe-based catalysts, Yang et al.[111] used alkali metal K and transition metal Mn as promoters to improve the light olefins selectivity of Fe-based catalysts. The CO_2 conversion of Fe−Mn−K catalysts at 300 °C was 42.3%, and the light olefin selectivity was 30.4%, of which the olefin selectivity of C_2^+ was even as high at 83.1%. Zepeda et al.[112] synthesized Fe−Mn catalysts with a high specific surface area by coprecipitation and supercritical drying. Mn promoted the dispersion of catalytically active phases and made Fe more susceptible to reduction and carburization, thus, enhancing the activity of Fe-based catalysts. When the Mn/Fe atomic ratio was 0.05, the catalyst was able to achieve 44.2% CO_2 conversion and 68% light olefin selectivity. Liang et al.[113] investigated the effect of Mn on the performance of Na/Fe catalysts, which inhibited carbon chain growth due to the interaction between Mn and Fe. Therefore, the favorable CO_2 conversion (38.6%) and low-carbon olefin selectivity (30.2%) were exhibited when Mn and Na were 5 and 1 wt %. Zhang et al.[114] investigated the structural effects of Mn on Fe species in the reaction. Since Fe_2O_3 is converted to Fe_5C_2 during the carburization reaction, Mn can promote the carburization reaction to take place. Kinetic studies further evidence that MnO_x accelerates CO generation, reduces the number of olefin adsorption sites, and inhibits secondary hydrogenation of low-carbon olefins and improvement of light olefin selectivity.

The advantage of Cu in the CO_2 hydrogenation catalytic system is that it can accelerate the RWGS reaction activity and inhibit methane production. Hence, Fe−Cu bimetallic catalysts have received widespread attention in the study of CO_2 hydrogenation for the preparation of light olefins. Wang et al.[115] investigated the CO_2 hydrogenation process over Fe−Cu bimetallic catalysts and the interaction between Fe and Cu. The hydrogenation of CO_2 over Fe−Cu catalysts was investigated by product distribution analysis and in situ drift in both direct and indirect ways. The direct pathway leads to the formation of more HCs, while the indirect pathway mainly produces CO as the main product. This in-depth study elucidates the complex process of CO_2 hydrogenation and provides important new information about the role of Fe−Cu bimetallic catalysts in the production of olefin-rich hydrocarbons. Choi et al.[116] synthesized $CuFeO_2$ catalysts by hydrothermal crystallization, the structure of which can accelerate the reduction and carburization of Cu for Fe-based catalysts, thus increasing the selectivity of olefins in the product, and thus O/P in the product reached 7.7. Chaipraditgul et al.[109] found that the addition of Cu to Fe/K−Al_2O_3 significantly increased the number of weakly adsorbed H atoms and thus improved the CO_2 conversion. Fe−Cu/K−Al_2O_3 catalyst achieved 36% CO_2 conversion and 44.2% light olefins selectivity at 340 °C, 20 bar. Nie et al.[58] investigated the energy level change of Cu−Fe catalysts for C−C coupling to produce ethylene by DFT calculations. When forming a Cu−x-Fe_5C_2 catalyst, it can reduce the binding energy of C−C coupling and speed up the reaction to increase the light olefins yield.

In summary, transition metals improve the activity of Fe-based catalysts by increasing the dispersion of Fe particles and forming interactions; Zn has a positive effect on inhibiting the further oxidation of the active phase Fe_5C_2 and the carbon deposition on the catalyst surface; it also has a positive effect on the dissociation of light olefins; Mn interacts positively with Fe to weaken the chain growth of Fe-based catalysts and improve the low carbon olefin selectivity; and Mn also promotes the reduction and carburization of Fe to improve the catalytic effect. selectivity, Mn also promotes the reduction and carburization of Fe to improve the catalytic effect; Cu can improve the RWGS reaction activity of Fe-based catalysts, and Cu facilitates the carburization of Fe to improve the light olefin selectivity.

3.4. Supports. The catalyst carrier is the dispersant, binder and support for the main catalyst and cocatalyst in the catalyst, and the catalytic carrier plays a key role in the service life of the catalyst.[117−119] Therefore, catalyst carriers with a high specific surface area can promote the dispersion of Fe and increase the number of reaction sites of the catalyst.

3.4.1. Oxide Supports. Metal−carrier interactions can be formed between metal oxides and Fe-based catalysts for better bonding of metal nanoparticles and improved catalyst lifetime.[120−122] It was shown that the high specific surface area of the ZrO_2 carrier could avoid the deactivation of Fe-based catalysts due to high-temperature sintering. Gu et al.[74] investigated the effect of different ZrO crystal phases on the performance of K/Fe catalysts, and the results are shown in

https://doi.org/10.1021/acsomega.4c03075
ACS Omega 2024, 9, 25610−25624

Figure 11a–c. The m-ZrO_2 has a higher oxygen vacancy concentration than t-ZrO_2, more oxygen vacancies on the m-

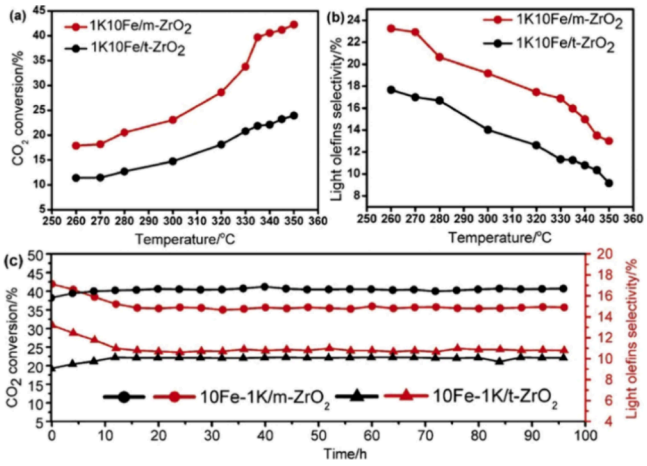

Figure 11. Performances of two samples for light olefins: (a) the conversion of CO_2; (b) the selectivity of light olefins; (c) the stability for 100 h at 340 °C. Reproduced with permission from ref 74. Copyright 2021 Elsevier.

ZrO_2 surface and the electron-donating ability of Fe promote charge transfer between Fe and ZrO_2 carriers the m-ZrO_2-loaded catalyst with a Fe/K molar ratio of 10/1 showed a CO_2 conversion of 40.5% and a light olefin selectivity of 14.9%. The redox-active carrier CeO_2 can change the nature of the catalysts to facilitate the reduction of FeO_x species without the use of promoters. Zhang et al.[72] added an appropriate amount of CeO_2 to the Fe–Zr–K catalyst, thereby increasing the catalyst surface alkalinity, reducing the particle size of Fe_2O_3, promoting the reduction of Fe, and dramatically improving the CO_2 conversion and light olefin selectivity.

The pore structure of the carrier also affects the diffusion of the feedstock and distribution of the products. Al_2O_3 is widely used as an effective carrier for CO_2 hydrogenation to light olefins, and its pore size not only affects the reducibility of Fe_2O_3, but also the selectivity of the products.[123] The larger pore size of Al_2O_3 is good for the reduction of Fe_2O_3 to metallic iron and promotes the CO_2 hydrogenation. Wang et al.[2] found that Al_2O_3 catalysts with larger pore sizes had lower diffusion resistance and therefore higher olefin yields (14.2%) than Al_2O_3 catalysts with smaller pore sizes (12.6%).

MgO and TiO_2 were also commonly used catalyst carriers for the preparation of low carbon olefins by CO_2 hydrogenation. The electron-donating property and surface alkalinity of MgO promoted the dissociation and adsorption of CO, limiting the hydrogenation ability of the Fe-based catalysts, while the stability of the basic sites effectively prevented the loss of the active substances and the basic sites during the reaction process, which improved the selectivity of light olefins.[124,125] XRD and CO_2-TPD measurements showed that the (111) crystalline facets of MgO increased the surface alkalinity of the catalyst, facilitated the dissociative adsorption of CO, and accelerated the reaction rate.[126,127] The oxygen vacancies in the TiO_2 carrier help bridge the adsorption of carbonate species and promote the decomposition of carbonate species into carbon intermediates, accelerating the C–C coupling reaction.[128]

In conclusion, the high specific surface area of ZrO_2 carrier can avoid the deactivation of iron-based catalysts due to high temperature sintering; CeO_2, MgO, and TiO_2 are used to increase the alkalinity of the catalyst surface and disperse the particle size of Fe to achieve the enhancement of catalytic activity; and the pore structure of Al_2O_3 affects the diffusion of raw materials to regulate the product distribution.

3.4.2. Carbon Supports. Compared with metal oxides, porous carbon materials with a larger specific surface area can effectively limit the migration and agglomeration of iron carbide nanoparticles and improve the stability of Fe-based catalysts.[129,130] Graphene and carbon nanotubes (CNTs) as representative carbon materials were often used as Fe-based catalyst carriers due to their outstanding structural features, including high specific surface area, abundant porosity, and specific nanostructures.

CNTs had a high mechanical strength, which was important for supporting Fe nanoparticles to extend the lifetime of the catalyst. Bao et al.[131] conducted the first detailed study on the application of CNTs in FTS, which laid the foundation for the subsequent use of CNTs as Fe catalyst carriers. It was found that the domain-limiting effect of CNTs could induce the self-reduction of iron oxides, while Fe_2O_3 encapsulated inside the CNTs was easier to reduce than Fe_2O_3 encapsulated outside the CNTs, which made the CNTs favorable for the formation of iron carbides. Kim et al.[77] prepared Na-$CoFe_2O_4$/CNTs catalysts, and CNTs facilitated the formation of a unique bimetallic alloy carbide $(Fe_{1-x}Co_x)_5C_2$ structure for Fe–Co catalysts, which was able to achieve 34% CO_2 conversion and 39% light hydrocarbon selectivity.

Graphene not only exhibited an ultrahigh specific surface area, but also a honeycomb structure that facilitated mass transfer and inhibited the agglomeration of iron carbide nanoparticles.[132,133] Wu et al.[134] showed that Fe-based catalysts with 3D porous graphene material loading had higher catalytic activity and selectivity for light olefins. The mesoporous structure of honeycomb graphene contained the agglomeration phenomenon of iron oxide nanoparticles and improved the dispersion degree of Fe-based catalysts. The highly dispersed Fe-based catalyst exhibited excellent light olefin selectivity (59%), and the honeycomb graphene material effectively avoided the sintering problem of Fe-based catalysts, which did not show any significant deactivation after 120 h of catalyst cycling. Peng et al.[135] showed through theoretical calculations that graphene as a carrier has high stability, which greatly changes the electron density on Fe–Co clusters and thus facilitates the coupling of C–C bonds. In addition, the dispersion of graphene carriers could obtain a narrow particle size distribution of Fe–Co catalysts, which resulted in 36% CO_2 conversion and 51% light olefin selectivity.

In conclusion, the rigidity of CNTs can support iron nanoparticles to extend the catalyst lifetime, and the CNTs facilitate the formation of iron carbide from Fe by carburization; The large specific surface area and three-dimensional porous structure of cellular graphene can accelerate mass transfer and inhibit the agglomeration of iron carbide nanoparticles

3.5. Preparation Method. In addition to the influence of alkali and transition metal promoters and carriers, the preparation method also affected the Fe-based catalyst properties. Albrecht et al.[136] compared Fe_2O_3–CT600 prepared by cellulose synthesis with Fe_2O_3–P prepared by coprecipitation. By Musburger spectroscopy, Fe_2O_3–CT600 has 80% carbides, whereas Fe_2O_3–P contains about 30%

https://doi.org/10.1021/acsomega.4c03075
ACS Omega 2024, 9, 25610–25624

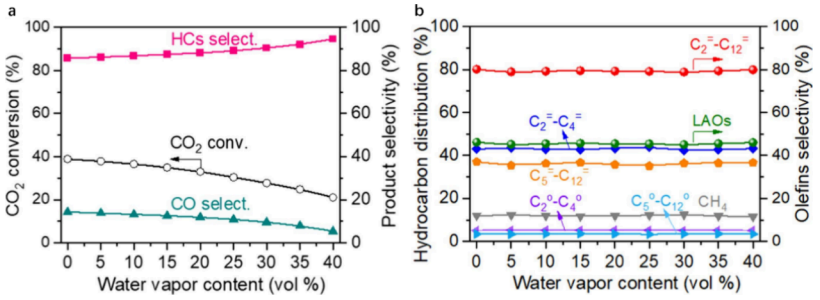

Figure 12. Effect of H_2O content on catalytic performances of Na−Zn−Fe catalyst for CO_2 and CO hydrogenation: (a) catalytic performances and (b) hydrocarbon distribution in CO_2 hydrogenation. Reproduced with permission from ref 138. Copyright 2020 Elsevier.

carbides, which leads to higher CO_2 conversion and olefin selectivity of Fe_2O_3−CT600.

For Fe-based catalysts, the calcination temperature could modulate the interaction between iron oxides and other metal oxides and carriers. Numpilai et al.[137] concluded that increasing the calcination temperature of Fe−Co−K/Al_2O_3 enhances the interaction of iron oxides with promoters and carriers, but at the same time inhibited the reduction of Fe-based catalysts and the formation of iron carbides. In addition, the length of the calcination time was also able to affect the structural phase of Fe-based catalysts, and the slow heating rate and long calcination time tended to form structurally stable Fe_2O_3, which was unfavorable to the reduction and carburization of Fe-based catalysts.

To summarize, Fe-based catalysts prepared by different methods have different reduction and carburization abilities, which leads to different iron carbide contents. High calcination temperatures and long calcination times favored the formation of structurally stable and difficult-to-reduce Fe_2O_3 catalysts.

3.6. The Effect of H_2O. As evidenced by the CO_2 hydrogenation reaction, the RWGS reaction produces the byproduct H_2O, which accelerated the oxidation of iron carbide and inhibited the RWGS reaction. Zhang et al.[138] investigated the CO_2 hydrogenation over Na−Zn−Fe catalysts at different H_2O contents. The results in Figure 12a,b show that with the increase of H_2O content from 0% to 40%, the CO_2 conversion and CO selectivity decreased significantly to 20% and 6%, respectively, while the product distribution remained unchanged. According to thermodynamic calculations, the equilibrium conversion of CO_2 was 60%, but currently reported CO_2 conversion rates are 30−50%. This was due to the fact that the H_2O produced during the RWGS reaction inhibited the activation of CO_2 and the properties of FeC_x, thus reducing the CO_2 conversion.[139] Guo et al.[140] used a multistage reactor for the removal of H_2O from the reaction system and achieved some results, and the Fe catalyst of the multistage reactor system achieved a CO_2 conversion rate of 69.9%. However, the high cost and consumption of multistage reactors are not advantageous for industrial-scale catalytic reactions.

Modification of iron-based catalysts with hydrophobic substances to accelerate the diffusion of H_2O generated on the catalyst surface is a promising strategy. Shi et al.[141] designed an iron-based catalyst with trimethylchlorosilane (TMCS) as the hydrophobic agent and polyvinylpyrrolidone (PVP)-modified Prussian blue (PB, $Fe_4[Fe(CN)_6]_3$) as precursor. The chemical reaction pathways were modulated by the hydrophobic surface of the catalysts, and a 48% selectivity for low-carbon olefins was achieved. Zhao et al.[142] achieved the preparation of hydrophobic iron-based catalysts by impregnating ferric ammonium citrate solution on expanded graphite (EG), a hydrophobic functional carbon material. Ferric ammonium citrate formed a smooth hydrophobic iron salt film on the surface of EG by high-temperature calcination, which was helpful in reducing the toxicity of H_2O during the catalytic process. The optimal results of this catalyst were 42.4% CO_2 conversion and 14.8% light olefin yield.

In summary, the design of multistage reactors can effectively remove H_2O to improve CO_2 conversion, but this approach has the disadvantage of high cost and cannot be industrialized; The iron-based catalyst modified with hydrophobic components or groups is an effective strategy for rapid diffusion of H_2O on the surface of the catalyst in order to improve catalytic stability.

4. CONCLUSIONS

In recent years, to realize CO_2 energy saving and emission reduction and alleviate the global energy crisis, several scholars have carried out a lot of research on the conversion and utilization of CO_2, and some progress has been made. In general, the preparation of low-carbon olefins from CO_2 by hydrogenation can be a new path for the continuous preparation of CH compounds. In this Review, the CO_2−Fischer−Tropsch method for the preparation of low-carbon olefins is introduced, and the reaction mechanism and catalytic system of the method are summarized.

In the CO_2−FTS route, Fe-based catalysts have the ability to accomplish CO_2 activation, H_2 activation, and C−C coupling at the same time, which has led to the deepening of research on Fe-based catalysts. Alkali metal promoters characterized by K and Na were generally effective in the reduction and carbonization of microscopic catalysts, and their alkaline character also facilitated CO_2 dissociation, adsorption, and iron phase carbonization; Transition metal promoters represented by Zn, Mn, and Cu tend to optimize the iron phase distribution of the catalysts and promote the reduction and carbonization of Fe-based catalysts. Metal oxides, which were commonly used as carriers for Fe-based catalysts, can form suitable metal−carrier interactions with Fe-based catalysts, thereby enhancing the catalytic effect; Porous carbon carriers exhibited better performance due to their diverse configurations, large specific surface area, and abundant surface defects; Different preparation methods and high-temperature treatment conditions predetermine that the performance of Fe-based catalysts may also differ to some extent; Fe-based catalysts were prone to agglomeration and water toxicity during the reaction process, which made the use of Fe-based catalysts very limited.

https://doi.org/10.1021/acsomega.4c03075
ACS Omega 2024, 9, 25610−25624

Therefore, in-depth studies on the preparation of Fe-based catalysts, the selection of carriers, and the control of reaction conditions with Fe-based catalysts are still needed. For example, (1) further studies are still needed on the nature of the active sites of the reaction catalysts, the interactions between the active components and the carriers, and the reaction mechanisms; (2) it is of practical significance to develop an all-in-one catalyst multifunctional catalyst with high catalytic activity by combining the RWGS and FTS reactions; (3) it is also important to effectively remove the water generated during the RWGS process to extend the catalyst life, ensure the catalyst activity, and improve the selectivity of low-carbon olefins in the product; (4) the combination of DFT calculations and in situ testing provides an in-depth analysis of the reaction history of Fe-based catalysts and the active sites of the catalysts, which can help to achieve catalyst modulation and large-scale application to industrial production.

AUTHOR INFORMATION

Corresponding Authors

Yongchun Zhang − *State Key Laboratory of Fine Chemicals, School of Chemical Engineering, Dalian University of Technology, 116024 Dalian, Liaoning, P.R. China;* orcid.org/0000-0001-7507-7297; Email: zhangyc@dlut.edu.cn

Chong Peng − *State Key Laboratory of Fine Chemicals, School of Chemical Engineering, Dalian University of Technology, 116024 Dalian, Liaoning, P.R. China;* orcid.org/0000-0002-0593-3083; Email: pengch@dlut.edu.cn

Author

Jiangtao Liu − *State Key Laboratory of Fine Chemicals, School of Chemical Engineering, Dalian University of Technology, 116024 Dalian, Liaoning, P.R. China;* orcid.org/0009-0001-0594-1665

Complete contact information is available at: https://pubs.acs.org/10.1021/acsomega.4c03075

Notes

The authors declare no competing financial interest.

ACKNOWLEDGMENTS

Natural Science Foundation of Shanghai (21ZR1425700); Fundamental Research Funds for the Central Universities (DUT23RC(3)044).

REFERENCES

(1) Ma, Z.; Porosoff, M. D. Development of Tandem Catalysts for CO_2 Hydrogenation to Olefins. *ACS Catal.* **2019**, *9*, 2639−2656.

(2) Wang, D.; Xie, Z.; Porosoff, M. D.; Chen, J. G. Recent Advances in Carbon Dioxide Hydrogenation to Produce Olefins and Aromatics. *Chem.* **2021**, *7*, 2277−2311.

(3) Posada-Pérez, S.; Ramírez, P. J.; Evans, J.; Viñes, F.; Liu, P.; Illas, F.; Rodriguez, J. A. Highly Active Au/Δ-Moc and Cu/Δ-Moc Catalysts for the Conversion of CO_2: The Metal/C Ratio as a Key Factor Defining Activity, Selectivity, and Stability. *J. Am. Chem. Soc.* **2016**, *138*, 8269−8278.

(4) Ji, G.; Yang, Z.; Zhang, H.; Zhao, Y.; Yu, B.; Ma, Z.; Liu, Z. Hierarchically Mesoporous O-Hydroxyazobenzene Polymers: Synthesis and Their Applications in CO_2 Capture and Conversion. *Angew. Chem., Int. Ed.* **2016**, *128*, 9837−9841.

(5) Ra, E. C.; Kim, K. Y.; Kim, E. H.; Lee, H.; An, K.; Lee, J. S. Recycling Carbon Dioxide through Catalytic Hydrogenation: Recent Key Developments and Perspectives. *ACS Catal.* **2020**, *10*, 11318−11345.

(6) Davis, S. J.; Caldeira, K.; Matthews, H. D. Future CO_2 Emissions and Climate Change from Existing Energy Infrastructure. *Science.* **2010**, *329*, 1330−1333.

(7) Sun, Y.; Hu, H.; Wang, Y.; Gao, J.; Tang, Y.; Wan, P.; Hu, Q.; Lv, J.; Zhang, T.; Yang, X. J. In Situ Hydrogenation of CO_2 by Al/Fe and Zn/Cu Alloy Catalysts under Mild Conditions. *Chem. Eng. Technol.* **2019**, *42*, 1223−1231.

(8) Wang, Y.; Kattel, S.; Gao, W.; Li, K.; Liu, P.; Chen, J. G.; Wang, H. Exploring the Ternary Interactions in Cu−Zno−ZrO_2 Catalysts for Efficient CO_2 Hydrogenation to Methanol. *Nat. Commun.* **2019**, *10*, 1166.

(9) Ni, Z.; Cai, M.; Zhong, S.; Chen, X.; Shen, H.; Su, L. Sodium Promoted Fezn@ SiO_2-C Catalysts for Sustainable Production of Low Olefins by CO_2 Hydrogenation. *Catalysts* **2023**, *13*, 1508.

(10) Yan, Y.; Dai, Y.; He, H.; Yu, Y.; Yang, Y. A Novel W-Doped Ni-Mg Mixed Oxide Catalyst for CO_2 Methanation. *Appl. Catal., B* **2016**, *196*, 108−116.

(11) Kothandaraman, J.; Goeppert, A.; Czaun, M.; Olah, G. A.; Prakash, G. S. Conversion of CO_2 from Air into Methanol Using a Polyamine and a Homogeneous Ruthenium Catalyst. *J. Am. Chem. Soc.* **2016**, *138*, 778−781.

(12) Saravanan, K.; Ham, H.; Tsubaki, N.; Bae, J. W. Recent Progress for Direct Synthesis of Dimethyl Ether from Syngas on the Heterogeneous Bifunctional Hybrid Catalysts. *Appl. Catal., B* **2017**, *217*, 494−522.

(13) Duan, R.; Qin, W.; Xiao, X.; Ma, B.; Zheng, Z. Influence of Ag Metal Dispersion on the Catalyzed Reduction of CO_2 into Chemical Fuels over Ag-ZrO_2 Catalysts. *ACS Omega* **2022**, *7*, 34213−34221.

(14) Weber, D.; Gandotra, A.; Schossig, J.; Zhang, H.; Wildy, M.; Wei, W.; Arizapana, K.; Zhang, J. Z.; Lu, P.; Zhang, C. Promoter Effect on Carbon Nanosphere-Encapsulated Fe-Co Catalysts for Converting CO_2 to Light Olefins. *Catalysts* **2023**, *13*, 1416.

(15) Álvarez, A.; Bansode, A.; Urakawa, A.; Bavykina, A. V.; Wezendonk, T. A.; Makkee, M.; Gascon, J.; Kapteijn, F. Challenges in the Greener Production of Formates/Formic Acid, Methanol, and Dme by Heterogeneously Catalyzed CO_2 Hydrogenation Processes. *Chem. Rev.* **2017**, *117*, 9804−9838.

(16) Jia, J.; Qian, C.; Dong, Y.; Li, Y. F.; Wang, H.; Ghoussoub, M.; Butler, K. T.; Walsh, A.; Ozin, G. A. Heterogeneous Catalytic Hydrogenation of CO_2 by Metal Oxides: Defect Engineering−Perfecting Imperfection. *Chem. Soc. Rev.* **2017**, *46*, 4631−4644.

(17) Kattel, S.; Liu, P.; Chen, J. G. Tuning Selectivity of CO_2 Hydrogenation Reactions at the Metal/Oxide Interface. *J. Am. Chem. Soc.* **2017**, *139*, 9739−9754.

(18) Yoshimura, Y.; Kijima, N.; Hayakawa, T.; Murata, K.; Suzuki, K.; Mizukami, F.; Matano, K.; Konishi, T.; Oikawa, T.; Saito, M.; et al. Catalytic Cracking of Naphtha to Light Olefins. *Catal. Surv. Jpn.* **2001**, *4*, 157−167.

(19) Longstaff, D. C. Development of a Comprehensive Naphtha Catalytic Cracking Kinetic Model. *Energy Fuels* **2012**, *26*, 801−809.

(20) Pyl, S. P.; Schietekat, C. M.; Reyniers, M.-F.; Abhari, R.; Marin, G. B.; Van Geem, K. M. Biomass to Olefins: Cracking of Renewable Naphtha. *Chem. Eng. J.* **2011**, *176*, 178−187.

(21) Bentley, R. W. Global Oil & Gas Depletion: An Overview. *Energy Policy* **2002**, *30*, 189−205.

(22) He, Y.; Liu, S.; Fu, W.; Wang, C.; Mebrahtu, C.; Sun, R.; Zeng, F. Thermodynamic Analysis of CO_2 Hydrogenation to Higher Alcohols ($C_{(2-4)}Oh$): Effects of Isomers and Methane. *ACS Omega* **2022**, *7*, 16502−16514.

(23) Ronda-Lloret, M.; Rothenberg, G.; Shiju, N. R. A Critical Look at Direct Catalytic Hydrogenation of Carbon Dioxide to Olefins. *ChemSusChem.* **2019**, *12*, 3896−3914.

(24) Ding, M.; Yang, Y.; Wu, B.; Li, Y.; Wang, T.; Ma, L. Study on Reduction and Carburization Behaviors of Iron Phases for Iron-Based Fischer−Tropsch Synthesis Catalyst. *Appl. Energy* **2015**, *160*, 982−989.

(25) Zhao, Z.; Chong, K.; Jiang, J.; Wilson, K.; Zhang, X.; Wang, F. Low-Carbon Roadmap of Chemical Production: A Case Study of Ethylene in China. *Renew.Sust. Energy Rev.* **2018**, *97*, 580−591.
(26) Xu, S.; Zhi, Y.; Han, J.; Zhang, W.; Wu, X.; Sun, T.; Wei, Y.; Liu, Z. Advances in Catalysis for Methanol-to-Olefins Conversion. *Adv. Catal.* **2017**, *61*, 37−122.
(27) Su, X.; Yang, X.; Zhao, B.; Huang, Y. Designing of Highly Selective and High-Temperature Endurable Rwgs Heterogeneous Catalysts: Recent Advances and the Future Directions. *J. Energy. Chem.* **2017**, *26*, 854−867.
(28) Daza, Y. A.; Kuhn, J. N. CO_2 Conversion by Reverse Water Gas Shift Catalysis: Comparison of Catalysts, Mechanisms and Their Consequences for CO_2 Conversion to Liquid Fuels. *RSC. Adv.* **2016**, *6*, 49675−49691.
(29) Orege, J. I.; Kifle, G. A.; Yu, Y.; Wei, J.; Ge, Q.; Sun, J. Emerging Spinel Ferrite Catalysts for Driving CO_2 Hydrogenation to High-Value Chemicals. *Matter* **2023**, *6*, 1404−1434.
(30) Jiang, F.; Liu, B.; Geng, S.; Xu, Y.; Liu, X. Hydrogenation of CO_2 into Hydrocarbons: Enhanced Catalytic Activity over Fe-Based Fischer−Tropsch Catalysts. *Catal. Sci. Technol.* **2018**, *8*, 4097−4107.
(31) Xu, M.; Cao, C.; Xu, J. Understanding Kinetically Interplaying Reverse Water-Gas Shift and Fischer−Tropsch Synthesis During CO_2 Hydrogenation over Fe-Based Catalysts. *Appl. Catal., A* **2022**, *641*, No. 118682.
(32) Sonal; Ahmad, E.; Upadhyayula, S.; Pant, K. K. Biomass-Derived CO_2 Rich Syngas Conversion to Higher Hydrocarbon Via Fischer−Tropsch Process over Fe−Co Bimetallic Catalyst. *Int. J. Hydrogen. Energy* **2019**, *44*, 27741−27748.
(33) Yang, H.; Zhang, C.; Gao, P.; Wang, H.; Li, X.; Zhong, L.; Wei, W.; Sun, Y. A Review of the Catalytic Hydrogenation of Carbon Dioxide into Value-Added Hydrocarbons. *Catal. Sci. Technol.* **2017**, *7*, 4580−4598.
(34) Abelló, S.; Montané, D. Exploring Iron-Based Multifunctional Catalysts for Fischer−Tropsch Synthesis: A Review. *ChemSusChem.* **2011**, *4*, 1538−1556.
(35) Čejka, J.; Centi, G.; Perez-Pariente, J.; Roth, W. J. Zeolite-Based Materials for Novel Catalytic Applications: Opportunities, Perspectives and Open Problems. *Cataly. Today* **2012**, *179*, 2−15.
(36) Wang, H.; Yang, Y.; Xu, J.; Wang, H.; Ding, M.; Li, Y. Study of Bimetallic Interactions and Promoter Effects of Fezn, Femn and Fecr Fischer−Tropsch Synthesis Catalysts. *J. Mol. Catal. A-chem.* **2010**, *326*, 29−40.
(37) Riedel, T.; Schulz, H.; Schaub, G.; Jun, K.-W.; Hwang, J.-S.; Lee, K.-W. Fischer−Tropsch on Iron with H_2/Co and H_2/ CO_2 as Synthesis Gases: The Episodes of Formation of the Fischer−Tropsch Regime and Construction of the Catalyst. *Top. Catal.* **2003**, *26*, 41−54.
(38) Puga, A. V. On the Nature of Active Phases and Sites in Co and CO_2 Hydrogenation Catalysts. *Catal. Sci. Technol.* **2018**, *8*, 5681−5707.
(39) Landau, M.; Meiri, N.; Utsis, N.; Vidruk Nehemya, R.; Herskowitz, M. Conversion of CO_2, CO, and H_2 in CO_2 Hydrogenation to Fungible Liquid Fuels on Fe-Based Catalysts. *Ind. Eng. Chem. Res.* **2017**, *56*, 13334−13355.
(40) Jiang, Y.; Wang, K.; Wang, Y.; Liu, Z.; Gao, X.; Zhang, J.; Ma, Q.; Fan, S.; Zhao, T.-S.; Yao, M. Recent Advances in Thermocatalytic Hydrogenation of Carbon Dioxide to Light Olefins and Liquid Fuels Via Modified Fischer−Tropsch Pathway. *J. CO_2 Util.* **2023**, *67*, No. 102321.
(41) Han, S. J.; Hwang, S.-M.; Park, H.-G.; Zhang, C.; Jun, K.-W.; Kim, S. K. Identification of Active Sites for CO_2 Hydrogenation in Fe Catalysts by First-Principles Microkinetic Modelling. *J. Mater. Chem. A* **2020**, *8*, 13014−13023.
(42) Gamba, O.; Noei, H.; Pavelec, J.; Bliem, R.; Schmid, M.; Diebold, U.; Stierle, A.; Parkinson, G. S. Adsorption of Formic Acid on the Fe_3O_4 (001) Surface. *J. Phys. Chem. C* **2015**, *119*, 20459−20465.
(43) Sun, S.-P.; Lemley, A. T. P-Nitrophenol Degradation by a Heterogeneous Fenton-Like Reaction on Nano-Magnetite: Process Optimization, Kinetics, and Degradation Pathways. *J. Mol. Catal. A-chem.* **2011**, *349*, 71−79.
(44) Estrella, M.; Barrio, L.; Zhou, G.; Wang, X.; Wang, Q.; Wen, W.; Hanson, J. C.; Frenkel, A. I.; Rodriguez, J. A. In Situ Characterization of $CuFe_2O_4$ and Cu/Fe_3O_4 Water− Gas Shift Catalysts. *J. Phys. Chem. C* **2009**, *113*, 14411−14417.
(45) Li, Y.; Chan, S. H.; Sun, Q. Heterogeneous Catalytic Conversion of CO_2: A Comprehensive Theoretical Review. *Nanoscale.* **2015**, *7*, 8663−8683.
(46) Kondratenko, E. V.; Mul, G.; Baltrusaitis, J.; Larrazábal, G. O.; Pérez-Ramírez, J. Status and Perspectives of CO_2 Conversion into Fuels and Chemicals by Catalytic, Photocatalytic and Electrocatalytic Processes. *Energy Environ. Sci.* **2013**, *6*, 3112−3135.
(47) Cheng, M.-J.; Clark, E. L.; Pham, H. H.; Bell, A. T.; Head-Gordon, M. Quantum Mechanical Screening of Single-Atom Bimetallic Alloys for the Selective Reduction of CO_2 to C1 Hydrocarbons. *ACS Catal.* **2016**, *6*, 7769−7777.
(48) Yang, X.; Kattel, S.; Senanayake, S. D.; Boscoboinik, J. A.; Nie, X.; Graciani, J.; Rodriguez, J. A.; Liu, P.; Stacchiola, D. J.; Chen, J. G. Low Pressure CO_2 Hydrogenation to Methanol over Gold Nanoparticles Activated on a Ceo X/TiO_2 Interface. *J. Am. Chem. Soc.* **2015**, *137*, 10104−10107.
(49) Zhang, Z.; Li, Y.; Hou, C.; Zhao, C.; Ke, Z. Dft Study of CO_2 Hydrogenation Catalyzed by a Cobalt-Based System: An Unexpected Formate Anion-Assisted Deprotonation Mechanism. *Catal. Sci. Technol.* **2018**, *8*, 656−666.
(50) Vasileff, A.; Xu, C.; Jiao, Y.; Zheng, Y.; Qiao, S.-Z. Surface and Interface Engineering in Copper-Based Bimetallic Materials for Selective CO_2 Electroreduction. *Chem.* **2018**, *4*, 1809−1831.
(51) Ojeda, M.; Nabar, R.; Nilekar, A. U.; Ishikawa, A.; Mavrikakis, M.; Iglesia, E. Co Activation Pathways and the Mechanism of Fischer−Tropsch Synthesis. *J. Catal.* **2010**, *272*, 287−297.
(52) Willauer, H. D.; Ananth, R.; Olsen, M. T.; Drab, D. M.; Hardy, D. R.; Williams, F. W. Modeling and Kinetic Analysis of CO_2 Hydrogenation Using a Mn and K-Promoted Fe Catalyst in a Fixed-Bed Reactor. *J. CO_2 Util.* **2013**, *3*, 56−64.
(53) Ojeda, M.; Li, A.; Nabar, R.; Nilekar, A. U.; Mavrikakis, M.; Iglesia, E. Kinetically Relevant Steps and H_2/D_2 Isotope Effects in Fischer− Tropsch Synthesis on Fe and Co Catalysts. *J. Phys. Chem. C* **2010**, *114*, 19761−19770.
(54) Bo, C.; Maseras, F.; López, N. The Role of Computational Results Databases in Accelerating the Discovery of Catalysts. *Nat. Catal.* **2018**, *1*, 809−810.
(55) Ko, J.; Kim, B.-K.; Han, J. W. Density Functional Theory Study for Catalytic Activation and Dissociation of CO_2 on Bimetallic Alloy Surfaces. *J. Phys. Chem. C* **2016**, *120*, 3438−3447.
(56) Gao, P.; Dang, S.; Li, S.; Bu, X.; Liu, Z.; Qiu, M.; Yang, C.; Wang, H.; Zhong, L.; Han, Y.; et al. Direct Production of Lower Olefins from CO_2 Conversion Via Bifunctional Catalysis. *ACS Catal.* **2018**, *8*, 571−578.
(57) Li, Z.; Wang, J.; Qu, Y.; Liu, H.; Tang, C.; Miao, S.; Feng, Z.; An, H.; Li, C. Highly Selective Conversion of Carbon Dioxide to Lower Olefins. *ACS Catal.* **2017**, *7*, 8544−8548.
(58) Nie, X.; Wang, H.; Janik, M. J.; Chen, Y.; Guo, X.; Song, C. Mechanistic Insight into C−C Coupling over Fe−Cu Bimetallic Catalysts in CO_2 Hydrogenation. *J. Phys. Chem. C* **2017**, *121*, 13164−13174.
(59) Liu, J.; Zhang, A.; Jiang, X.; Liu, M.; Sun, Y.; Song, C.; Guo, X. Selective CO_2 Hydrogenation to Hydrocarbons on Cu-Promoted Fe-Based Catalysts: Dependence on Cu−Fe Interaction. *Acs Sustain. Chem. Eng.* **2018**, *6*, 10182−10190.
(60) Wang, J.; Bai, Z. Fe-Based Catalysts for Heterogeneous Catalytic Ozonation of Emerging Contaminants in Water and Wastewater. *Chem. Eng. J.* **2017**, *312*, 79−98.
(61) Liu, J.; Peng, C.; Shi, X. Preparation, Characterization, and Applications of Fe-Based Catalysts in Advanced Oxidation Processes for Organics Removal: A Review. *Environ. Pollut.* **2022**, *293*, No. 118565.

https://doi.org/10.1021/acsomega.4c03075
ACS Omega 2024, 9, 25610−25624

(62) Jaouen, F.; Charreteur, F.; Dodelet, J. Fe-Based Catalysts for Oxygen Reduction in Pemfcs: Importance of the Disordered Phase of the Carbon Support. *J. Electrochem. Soc.* **2006**, *153*, A689.
(63) Medard, C.; Lefevre, M.; Dodelet, J.; Jaouen, F.; Lindbergh, G. Oxygen Reduction by Fe-Based Catalysts in Pem Fuel Cell Conditions: Activity and Selectivity of the Catalysts Obtained with Two Fe Precursors and Various Carbon Supports. *Electrochim. Acta* **2006**, *51*, 3202−3213.
(64) Xu, Y.; Shi, C.; Liu, B.; Wang, T.; Zheng, J.; Li, W.; Liu, D.; Liu, X. Selective Production of Aromatics from CO_2. *Catal. Sci. Technol.* **2019**, *9*, 593−610.
(65) Liu, B.; Geng, S.; Zheng, J.; Jia, X.; Jiang, F.; Liu, X. Unravelling the New Roles of Na and Mn Promoter in CO_2 Hydrogenation over Fe_3O_4-Based Catalysts for Enhanced Selectivity to Light A-Olefins. *ChemCatChem.* **2018**, *10*, 4718−4732.
(66) Wei, J.; Sun, J.; Wen, Z.; Fang, C.; Ge, Q.; Xu, H. New Insights into the Effect of Sodium on Fe_3O_4-Based Nanocatalysts for CO_2 Hydrogenation to Light Olefins. *Catal. Sci. Technol.* **2016**, *6*, 4786−4793.
(67) YOU, Z.; DENG, W.; ZHANG, Q.; WANG, Y. Hydrogenation of Carbon Dioxide to Light Olefins over Non-Supported Iron Catalyst. *Chinese. J. Catal.* **2013**, *34*, 956−963.
(68) Meiri, N.; Dinburg, Y.; Amoyal, M.; Koukouliev, V.; Nehemya, R. V.; Landau, M. V.; Herskowitz, M. Novel Process and Catalytic Materials for Converting CO_2 and H_2 Containing Mixtures to Liquid Fuels and Chemicals. *Faraday Discuss.* **2015**, *183*, 197−215.
(69) Malhi, H. S.; Sun, C.; Zhang, Z.; liu, Y.; Liu, W.; Ren, P.; Tu, W.; Han, Y.-F. Catalytic Consequences of the Decoration of Sodium and Zinc Atoms During CO_2 Hydrogenation to Olefins over Iron-Based Catalyst. *Catal. Today* **2022**, *387*, 28−37.
(70) Zhang, J.; Lu, S.; Su, X.; Fan, S.; Ma, Q.; Zhao, T. Selective Formation of Light Olefins from CO_2 Hydrogenation over Fe−Zn−K Catalysts. *J. CO_2 Util.* **2015**, *12*, 95−100.
(71) Liu, J.; Zhang, A.; Liu, M.; Hu, S.; Ding, F.; Song, C.; Guo, X. Fe-Mof-Derived Highly Active Catalysts for Carbon Dioxide Hydrogenation to Valuable Hydrocarbons. *J. CO_2 Util.* **2017**, *21*, 100−107.
(72) Zhang, J.; Su, X.; Wang, X.; Ma, Q.; Fan, S.; Zhao, T.-S. Promotion Effects of Ce Added Fe−Zr−K on CO_2 Hydrogenation to Light Olefins. *React. Kinet. Mech. Catal.* **2018**, *124*, 575−585.
(73) Liu, J.; Zhang, A.; Jiang, X.; Liu, M.; Zhu, J.; Song, C.; Guo, X. Direct Transformation of Carbon Dioxide to Value-Added Hydrocarbons by Physical Mixtures of Fe_5C_2 and K-Modified Al_2O_3. *Ind. Eng. Chem. Res.* **2018**, *57*, 9120−9126.
(74) Gu, H.; Ding, J.; Zhong, Q.; Zeng, Y.; Song, F. Promotion of Surface Oxygen Vacancies on the Light Olefins Synthesis from Catalytic CO_2 Hydrogenation over FeK/ZrO_2 Catalysts. *Int. J. Hydrogen. Energy* **2019**, *44*, 11808−11816.
(75) Da Silva, I. A.; Mota, C. J. Conversion of CO_2 to Light Olefins over Iron-Based Catalysts Supported on Niobium Oxide. *Front. Energy Res.* **2019**, *7*, 49.
(76) Liu, J.; Sun, Y.; Jiang, X.; Zhang, A.; Song, C.; Guo, X. Pyrolyzing ZIF-8 to N-Doped Porous Carbon Facilitated by Iron and Potassium for CO_2 Hydrogenation to Value-Added Hydrocarbons. *J. CO_2 Util.* **2018**, *25*, 120−127.
(77) Kim, K. Y.; Lee, H.; Noh, W. Y.; Shin, J.; Han, S. J.; Kim, S. K.; An, K.; Lee, J. S. Cobalt Ferrite Nanoparticles to Form a Catalytic Co−Fe Alloy Carbide Phase for Selective CO_2 Hydrogenation to Light Olefins. *ACS Catal.* **2020**, *10*, 8660−8671.
(78) Feng, D.; Dong, Y.; Zhang, L.; Ge, X.; Zhang, W.; Dai, S.; Qiao, Z. A. Holey Lamellar High-Entropy Oxide as an Ultra-High-Activity Heterogeneous Catalyst for Solvent-Free Aerobic Oxidation of Benzyl Alcohol. *Angew. Chem., Int. Ed.* **2020**, *132*, 19671−19677.
(79) Migowski, P.; Dupont, J. Catalytic Applications of Metal Nanoparticles in Imidazolium Ionic Liquids. *Chem.—Eur. J.* **2007**, *13*, 32−39.
(80) Moro-Oka, Y.; Ueda, W. Multicomponent Bismuth Molybdate Catalyst: A Highly Functionalized Catalyst System for the Selective Oxidation of Olefin. *Adv. Catal.* **1994**, *40*, 233−273.
(81) Morris, R. V.; Lauer, H. V., Jr; Lawson, C. A.; Gibson, E. K., Jr; Nace, G. A.; Stewart, C. Spectral and Other Physicochemical Properties of Submicron Powders of Hematite (A-Fe_2O_3), Maghemite (Γ-Fe_2O_3), Magnetite (Fe_3O_4), Goethite (A-Feooh), and Lepidocrocite (Γ-Feooh). *J. Geophys. Res-Sol. Ea.* **1985**, *90*, 3126−3144.
(82) Zhang, Y.; Fu, D.; Liu, X.; Zhang, Z.; Zhang, C.; Shi, B.; Xu, J.; Han, Y. F. Operando Spectroscopic Study of Dynamic Structure of Iron Oxide Catalysts During CO_2 Hydrogenation. *ChemCatChem.* **2018**, *10*, 1272−1276.
(83) Ye, D.; Tang, W.; Zhang, T.; Lv, L.; Zou, Z.; Gupta, R. K.; Tang, S. Enhancing the Synergism of Fe_3O_4 and Fe_5C_2 to Improve the Process of CO_2 Hydrogenation to Olefines. *Colloid. Surfaces A* **2022**, *654*, No. 130145.
(84) Tang, L.; He, L.; Wang, Y.; Chen, B.; Xu, W.; Duan, X.; Lu, A.-H. Selective Fabrication of X-Fe_5C_2 by Interfering Surface Reactions as a Highly Efficient and Stable Fischer−Tropsch Synthesis Catalyst. *Appl. Catal., B* **2021**, *284*, No. 119753.
(85) Wang, Y.; Zhou, Y.; Zhang, X.; Wang, M.; Liu, T.; Wei, J.; Zhang, G.; Hong, X.; Liu, G. Pdfe Alloy- Fe_5C_2 Interfaces for Efficient CO_2 Hydrogenation to Higher Alcohols. *Applied Catalysis B: Environment and Energy* **2024**, *345*, No. 123691.
(86) Liu, Y.; Murthy, P. R.; Zhang, X.; Wang, H.; Shi, C. Phase Transformation of Iron Oxide to Carbide and Fe_3C as an Active Center for the Rwgs Reaction. *New.J. Chem.* **2021**, *45*, 22444−22449.
(87) Liu, J.; Li, K.; Song, Y.; Song, C.; Guo, X. Selective Hydrogenation of CO_2 to Hydrocarbons: Effects of Fe_3O_4 Particle Size on Reduction, Carburization, and Catalytic Performance. *Energy Fuels* **2021**, *35*, 10703−10709.
(88) Zhou, W.; Cheng, K.; Kang, J.; Zhou, C.; Subramanian, V.; Zhang, Q.; Wang, Y. New Horizon in C1 Chemistry: Breaking the Selectivity Limitation in Transformation of Syngas and Hydrogenation of CO_2 into Hydrocarbon Chemicals and Fuels. *Chem. Soc. Rev.* **2019**, *48*, 3193−3228.
(89) Lu, J.; Yang, L.; Xu, B.; Wu, Q.; Zhang, D.; Yuan, S.; Zhai, Y.; Wang, X.; Fan, Y.; Hu, Z. Promotion Effects of Nitrogen Doping into Carbon Nanotubes on Supported Iron Fischer−Tropsch Catalysts for Lower Olefins. *ACS Catal.* **2014**, *4*, 613−621.
(90) Jiang, F.; Zhang, M.; Liu, B.; Xu, Y.; Liu, X. Insights into the Influence of Support and Potassium or Sulfur Promoter on Iron-Based Fischer−Tropsch Synthesis: Understanding the Control of Catalytic Activity, Selectivity to Lower Olefins, and Catalyst Deactivation. *Catal. Sci. Technol.* **2017**, *7*, 1245−1265.
(91) Arcadi, A. Alternative Synthetic Methods through New Developments in Catalysis by Gold. *Chem. Rev.* **2008**, *108*, 3266−3325.
(92) Masters, C. *Homogeneous Transition-Metal Catalysis: A Gentle Art*; Springer Science & Business Media, 2012.
(93) Pospech, J.; Fleischer, I.; Franke, R.; Buchholz, S.; Beller, M. Alternative Metals for Homogeneous Catalyzed Hydroformylation Reactions. *Angew. Chem., Int. Ed.* **2013**, *52*, 2852−2872.
(94) Satthawong, R.; Koizumi, N.; Song, C.; Prasassarakich, P. Bimetallic Fe−Co Catalysts for CO_2 Hydrogenation to Higher Hydrocarbons. *J. CO_2 Util.* **2013**, *3*, 102−106.
(95) Wang, J.; You, Z.; Zhang, Q.; Deng, W.; Wang, Y. Synthesis of Lower Olefins by Hydrogenation of Carbon Dioxide over Supported Iron Catalysts. *Cataly. Today* **2013**, *215*, 186−193.
(96) Han, Y.; Fang, C.; Ji, X.; Wei, J.; Ge, Q.; Sun, J. Interfacing with Carbonaceous Potassium Promoters Boosts Catalytic CO_2 Hydrogenation of Iron. *ACS Catal.* **2020**, *10*, 12098−12108.
(97) Numpilai, T.; Chanlek, N.; Poo-Arporn, Y.; Cheng, C. K.; Siri-Nguan, N.; Sornchamni, T.; Chareonpanich, M.; Kongkachuichay, P.; Yigit, N.; Rupprechter, G.; et al. Tuning Interactions of Surface-Adsorbed Species over Fe−Co/K−Al_2O_3 Catalyst by Different K Contents: Selective CO_2 Hydrogenation to Light Olefins. *ChemCatChem.* **2020**, *12*, 3306−3320.
(98) Jiang, M.; Koizumi, N.; Yamada, M. Characterization of Potassium-Promoted Iron−Manganese Catalysts by Insitu Diffuse Reflectance Ftir Using NO, CO and CO+ H_2 as Probes. *Appl. Catal., A* **2000**, *204*, 49−58.

https://doi.org/10.1021/acsomega.4c03075
ACS Omega 2024, 9, 25610−25624

(99) Wang, Y.; Hu, P.; Yang, J.; Zhu, Y.-A.; Chen, D. C−H Bond Activation in Light Alkanes: A Theoretical Perspective. *Chem. Soc. Rev.* **2021**, *50*, 4299−4358.
(100) Tu, W.; Sun, C.; Zhang, Z.; Liu, W.; Malhi, H. S.; Ma, W.; Zhu, M.; Han, Y.-F. Chemical and Structural Properties of Na Decorated Fe_5C_2-Zno Catalysts During Hydrogenation of CO_2 to Linear A-Olefins. *Appl. Catal., B* **2021**, *298*, No. 120567.
(101) Liang, B.; Duan, H.; Sun, T.; Ma, J.; Liu, X.; Xu, J.; Su, X.; Huang, Y.; Zhang, T. Effect of Na Promoter on Fe-Based Catalyst for CO_2 Hydrogenation to Alkenes. *Acs Sustain. Chem. Eng.* **2019**, *7*, 925−932.
(102) Wei, C.; Tu, W.; Jia, L.; Liu, Y.; Lian, H.; Wang, P.; Zhang, Z. The Evolutions of Carbon and Iron Species Modified by Na and Their Tuning Effect on the Hydrogenation of CO_2 to Olefins. *Appl. Surf. Sci.* **2020**, *525*, No. 146622.
(103) Fu, C.; Qi, X.; Zhao, L.; Yang, T.; Xue, Q.; Zhu, Z.; Xiong, P.; Jiang, J.; An, X.; Chen, H.; et al. Synergistic Cooperation between Atomically Dispersed Zn and Fe on Porous Nitrogen-Doped Carbon for Boosting Oxygen Reduction Reaction. *Appl. Catal., B* **2023**, *335*, No. 122875.
(104) Liu, T.; Xu, D.; Wu, D.; Liu, G.; Hong, X. Spinel $ZnFe_2O_4$ Regulates Copper Sites for CO_2 Hydrogenation to Methanol. *Acs Sustain. Chem. Eng.* **2021**, *9*, 4033−4041.
(105) Yang, H.; Dang, Y.; Cui, X.; Bu, X.; Li, J.; Li, S.; Sun, Y.; Gao, P. Selective Synthesis of Olefins Via CO_2 Hydrogenation over Transition-Metal-Doped Iron-Based Catalysts. *Appl. Catal., B* **2023**, *321*, No. 122050.
(106) Zhang, Z.; Yin, H.; Yu, G.; He, S.; Kang, J.; Liu, Z.; Cheng, K.; Zhang, Q.; Wang, Y. Selective Hydrogenation of CO_2 and CO into Olefins over Sodium-and Zinc-Promoted Iron Carbide Catalysts. *J. Catal.* **2021**, *395*, 350−361.
(107) Zhang, C.; Xu, M.; Yang, Z.; Zhu, M.; Gao, J.; Han, Y.-F. Uncovering the Electronic Effects of Zinc on the Structure of Fe_5C_2-ZnO Catalysts for CO_2 Hydrogenation to Linear A-Olefins. *Appl. Catal., B* **2021**, *295*, No. 120287.
(108) Yao, B.; Xiao, T.; Makgae, O. A.; Jie, X.; Gonzalez-Cortes, S.; Guan, S.; Kirkland, A. I.; Dilworth, J. R.; Al-Megren, H. A.; Alshihri, S. M.; et al. Transforming Carbon Dioxide into Jet Fuel Using an Organic Combustion-Synthesized Fe-Mn-K Catalyst. *Nat. Commun.* **2020**, *11*, 6395.
(109) Chaipraditgul, N.; Numpilai, T.; Cheng, C. K.; Siri-Nguan, N.; Sornchamni, T.; Wattanakit, C.; Limtrakul, J.; Witoon, T. Tuning Interaction of Surface-Adsorbed Species over Fe/K-Al_2O_3 Modified with Transition Metals (Cu, Mn, V, Zn or Co) on Light Olefins Production from CO_2 Hydrogenation. *Fuel* **2021**, *283*, No. 119248.
(110) Fedorov, A.; Lund, H.; Kondratenko, V. A.; Kondratenko, E. V.; Linke, D. Elucidating Reaction Pathways Occurring in CO_2 Hydrogenation over Fe-Based Catalysts. *Appl. Catal., B* **2023**, *328*, No. 122505.
(111) Yang, Q.; Skrypnik, A.; Matvienko, A.; Lund, H.; Holena, M.; Kondratenko, E. V. Revealing Property-Performance Relationships for Efficient CO_2 Hydrogenation to Higher Hydrocarbons over Fe-Based Catalysts: Statistical Analysis of Literature Data and Its Experimental Validation. *Appl. Catal., B* **2021**, *282*, No. 119554.
(112) Zepeda, T. A.; Aguirre, S.; Galindo-Ortega, Y. I.; Solís-Garcia, A.; Navarro Yerga, R. M.; Pawelec, B.; Fierro-Gonzalez, J. C.; Fuentes, S. Hydrogenation of CO_2 to Valuable C_2-C_5 Hydrocarbons on Mn-Promoted High-Surface-Area Iron Catalysts. *Catalysts.* **2023**, *13*, 954.
(113) Liang, B.; Sun, T.; Ma, J.; Duan, H.; Li, L.; Yang, X.; Zhang, Y.; Su, X.; Huang, Y.; Zhang, T. Mn Decorated Na/Fe Catalysts for CO_2 Hydrogenation to Light Olefins. *Catal. Sci. Technol.* **2019**, *9*, 456−464.
(114) Zhang, Z.; Wei, C.; Jia, L.; Liu, Y.; Sun, C.; Wang, P.; Tu, W. Insights into the Regulation of Fena Catalysts Modified by Mn Promoter and Their Tuning Effect on the Hydrogenation of CO_2 to Light Olefins. *J. Catal.* **2020**, *390*, 12−22.
(115) Wang, W.; Wang, X.; Zhang, G.; Wang, K.; Zhang, F.; Yan, T.; Miller, J. T.; Guo, X.; Song, C. CO_2 Hydrogenation to Olefin-Rich Hydrocarbons over Fe-Cu Bimetallic Catalysts: An Investigation of Fe-Cu Interaction and Surface Species. *Front. Chem. Eng.* **2021**, *3*, No. 708014.
(116) Choi, Y. H.; Jang, Y. J.; Park, H.; Kim, W. Y.; Lee, Y. H.; Choi, S. H.; Lee, J. S. Carbon Dioxide Fischer−Tropsch Synthesis: A New Path to Carbon-Neutral Fuels. *Appl. Catal., B* **2017**, *202*, 605−610.
(117) Herranz, T.; Rojas, S.; Pérez-Alonso, F.; Ojeda, M.; Terreros, P.; Fierro, J. Hydrogenation of Carbon Oxides over Promoted Fe-Mn Catalysts Prepared by the Microemulsion Methodology. *Appl. Catal., A* **2006**, *311*, 66−75.
(118) Argyle, M. D.; Bartholomew, C. H. Heterogeneous Catalyst Deactivation and Regeneration: A Review. *Catalysts.* **2015**, *5*, 145−269.
(119) Mitchell, S.; Michels, N.-L.; Pérez-Ramírez, J. From Powder to Technical Body: The Undervalued Science of Catalyst Scale Up. *Chem. Soc. Rev.* **2013**, *42*, 6094−6112.
(120) Fu, W.; Yi, J.; Cheng, M.; Liu, Y.; Zhang, G.; Li, L.; Du, L.; Li, B.; Wang, G.; Yang, X. When Bimetallic Oxides and Their Complexes Meet Fenton-Like Process. *J. Hazard. Mater.* **2022**, *424*, No. 127419.
(121) Huang, B.; Wu, Z.; Zhou, H.; Li, J.; Zhou, C.; Xiong, Z.; Pan, Z.; Yao, G.; Lai, B. Recent Advances in Single-Atom Catalysts for Advanced Oxidation Processes in Water Purification. *J. Hazard. Mater.* **2021**, *412*, No. 125253.
(122) Li, T.; Peng, X.; Cui, P.; Shi, G.; Yang, W.; Chen, Z.; Huang, Y.; Chen, Y.; Peng, J.; Zou, R.; et al. Recent Progress and Future Perspectives of Flexible Metal-Air Batteries. *SmartMater.* **2021**, *2*, 519−553.
(123) Wang, Y.; Li, H.-X.; Li, X.-G.; Chen, D.; Xiao, W.-D. Effective Iron Catalysts Supported on Mixed Mgo−Al_2O_3 for Fischer−Tropsch Synthesis to Olefins. *Ind. Eng. Chem. Res.* **2020**, *59*, 11462−11474.
(124) Liu, K.; Xu, D.; Fan, H.; Hou, G.; Li, Y.; Huang, S.; Ding, M. Development of Mg-Modified Fe-Based Catalysts for Low-Concentration CO_2 Hydrogenation to Olefins. *ACS Sustain. Chem. Eng.* **2024**, *12*, 2070−2079.
(125) Ahmed, S.; Irshad, M.; Yoon, W.; Karanwal, N.; Sugiarto, J. R.; Khan, M. K.; Kim, S. K.; Kim, J. Evaluation of MgO as a Promoter for the Hydrogenation of CO_2 to Long-Chain Hydrocarbons over Fe-Based Catalysts. *Appl. Catal., B* **2023**, *338*, No. 123052.
(126) Hu, P.; Wang, S.; Zhuo, Y. CO_2 Adsorption Enhancement over Alkaline Metal-Promoted Mgo with SO_2, O_2, and H_2O Present: A Theoretical Study. *Sep. Purif. Technol.* **2022**, *284*, No. 120253.
(127) Liu, H.; Li, K.; Zhang, R.; Ling, L.; Wang, B. Insight into Carbon Deposition Associated with Nico/Mgo Catalyzed CH_4/CO_2 Reforming by Using Density Functional Theory. *Appl. Surf. Sci.* **2017**, *423*, 1080−1089.
(128) Boreriboon, N.; Jiang, X.; Song, C.; Prasassarakich, P. Fe-Based Bimetallic Catalysts Supported on TiO_2 for Selective CO_2 Hydrogenation to Hydrocarbons. *J. CO_2 Util.* **2018**, *25*, 330−337.
(129) Roberts, A. D.; Li, X.; Zhang, H. Porous Carbon Spheres and Monoliths: Morphology Control, Pore Size Tuning and Their Applications as Li-Ion Battery Anode Materials. *Chem. Soc. Rev.* **2014**, *43*, 4341−4356.
(130) Li, Z.; Guo, D.; Liu, Y.; Wang, H.; Wang, L. Recent Advances and Challenges in Biomass-Derived Porous Carbon Nanomaterials for Supercapacitors. *Chem. Eng. J.* **2020**, *397*, No. 125418.
(131) Chen, W.; Pan, X.; Willinger, M.-G.; Su, D. S.; Bao, X. Facile Autoreduction of Iron Oxide/Carbon Nanotube Encapsulates. *J. Am. Chem. Soc.* **2006**, *128*, 3136−3137.
(132) Li, R.; Li, Y.; Li, Z.; Wei, W.; Hao, Q.; Shi, Y.; Ouyang, S.; Yuan, H.; Zhang, T. Electronically Activated Fe_5C_2 Via N-Doped Carbon to Enhance Photothermal Syngas Conversion to Light Olefins. *ACS Catal.* **2022**, *12*, 5316−5326.
(133) Chen, Y.; Wei, J.; Duyar, M. S.; Ordomsky, V. V.; Khodakov, A. Y.; Liu, J. Carbon-Based Catalysts for Fischer−Tropsch Synthesis. *Chem. Soc. Rev.* **2021**, *50*, 2337−2366.
(134) Wu, T.; Lin, J.; Cheng, Y.; Tian, J.; Wang, S.; Xie, S.; Pei, Y.; Yan, S.; Qiao, M.; Xu, H.; et al. Porous Graphene-Confined Fe−K as Highly Efficient Catalyst for CO_2 Direct Hydrogenation to Light Olefins. *ACS Appl. Mater. Interfaces.* **2018**, *10*, 23439−23443.

https://doi.org/10.1021/acsomega.4c03075
ACS Omega 2024, 9, 25610−25624

(135) Peng, L.; Jurca, B.; Primo, A.; Gordillo, A.; Parvulescu, V. I.; García, H. High C_2-C_4 Selectivity in CO_2 Hydrogenation by Particle Size Control of Co-Fe Alloy Nanoparticles Wrapped on N-Doped Graphitic Carbon. *Iscience* **2022**, *25*, 104252.
(136) Albrecht, M.; Rodemerck, U.; Schneider, M.; Bröring, M.; Baabe, D.; Kondratenko, E. V. Unexpectedly Efficient CO_2 Hydrogenation to Higher Hydrocarbons over Non-Doped Fe_2O_3. *Appl. Catal., B* **2017**, *204*, 119−126.
(137) Numpilai, T.; Witoon, T.; Chanlek, N.; Limphirat, W.; Bonura, G.; Chareonpanich, M.; Limtrakul, J. Structure−Activity Relationships of Fe-Co/K-Al_2O_3 Catalysts Calcined at Different Temperatures for CO_2 Hydrogenation to Light Olefins. *Appl. Catal., A* **2017**, *547*, 219−229.
(138) Zhang, Z.; Huang, G.; Tang, X.; Yin, H.; Kang, J.; Zhang, Q.; Wang, Y. Zn and Na Promoted Fe Catalysts for Sustainable Production of High-Valued Olefins by CO_2 Hydrogenation. *Fuel.* **2022**, *309*, No. 122105.
(139) Wang, K.; Peng, X.; Wang, C.; Gao, W.; Liu, N.; Guo, X.; He, Y.; Yang, G.; Jiang, L.; Tsubaki, N. Selective Direct Conversion of Aqueous Ethanol into Butadiene Via Rational Design of Multifunctional Catalysts. *Catal. Sci. Technol.* **2022**, *12*, 2210−2222.
(140) Guo, L.; Cui, Y.; Zhang, P.; Peng, X.; Yoneyama, Y.; Yang, G.; Tsubaki, N. Enhanced Liquid Fuel Production from Co2 Hydrogenation: Catalytic Performance of Bimetallic Catalysts over a Two-Stage Reactor System. *ChemistrySelect* **2018**, *3*, 13705−13711.
(141) Shi, Y.; Li, Z.; Hao, Q.; Li, R.; Li, Y.; Guo, L.; Ouyang, S.; Yuan, H.; Zhang, T. Hydrophobic Fe-Based Catalyst Derived from Prussian Blue for Enhanced Photothermal Conversion of Syngas to Light Olefins. *Adv. Funct. Mater.* **2024**, *34*, No. 2308670.
(142) Zhao, R.; Meng, X.; Yin, Q.; Gao, W.; Dai, W.; Jin, D.; Xu, B.; Xin, Z. Effect of Precursors of Fe-Based Fischer−Tropsch Catalysts Supported on Expanded Graphite for CO_2 Hydrogenation. *Acs Sustain. Chem. Eng.* **2021**, *9*, 15545−15556.

https://doi.org/10.1021/acsomega.4c03075
ACS Omega 2024, 9, 25610−25624